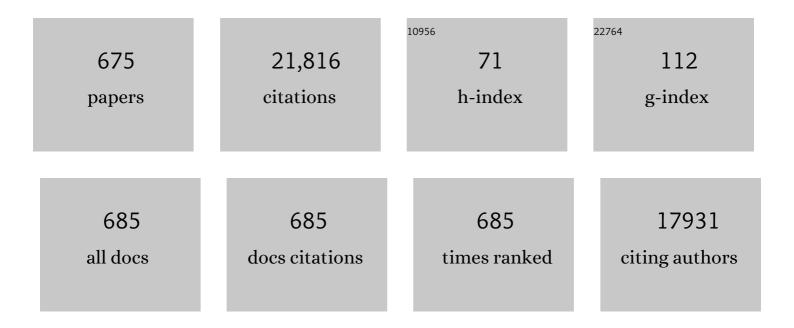
David J Smith

List of Publications by Year in descending order

Source: https://exaly.com/author-pdf/1129671/publications.pdf Version: 2024-02-01



ΠΛΛΙΟ Ι SMITH

#	Article	IF	CITATIONS
1	Bulk Production of a New Form of sp ² Carbon: Crystalline Graphene Nanoribbons. Nano Letters, 2008, 8, 2773-2778.	4.5	588
2	Giant magnetoresistance in antiferromagnetic Co/Cu multilayers. Applied Physics Letters, 1991, 58, 2710-2712.	1.5	582
3	Ex-MWNTs: Graphene Sheets and Ribbons Produced by Lithium Intercalation and Exfoliation of Carbon Nanotubes. Nano Letters, 2009, 9, 1527-1533.	4.5	369
4	Urine Steroid Metabolomics as a Biomarker Tool for Detecting Malignancy in Adrenal Tumors. Journal of Clinical Endocrinology and Metabolism, 2011, 96, 3775-3784.	1.8	369
5	Covalently bonded three-dimensional carbon nanotube solids via boron induced nanojunctions. Scientific Reports, 2012, 2, 363.	1.6	329
6	An investigation of grain boundaries in submicrometer-grained Al-Mg solid solution alloys using high-resolution electron microscopy. Journal of Materials Research, 1996, 11, 1880-1890.	1.2	317
7	Direct surface imaging in small metal particles. Nature, 1983, 303, 316-317.	13.7	250
8	Human spermatozoa migration in microchannels reveals boundary-following navigation. Proceedings of the United States of America, 2012, 109, 8007-8010.	3.3	247
9	Ge–Sn semiconductors for band-gap and lattice engineering. Applied Physics Letters, 2002, 81, 2992-2994.	1.5	237
10	Observation of ferromagnetism above 900K in Cr–GaN and Cr–AlN. Applied Physics Letters, 2004, 85, 4076-4078.	1.5	207
11	Nitrogen-Mediated Carbon Nanotube Growth: Diameter Reduction, Metallicity, Bundle Dispersability, and Bamboo-like Structure Formation. ACS Nano, 2007, 1, 369-375.	7.3	207
12	Heterodoped Nanotubes: Theory, Synthesis, and Characterization of Phosphorusâ^'Nitrogen Doped Multiwalled Carbon Nanotubes. ACS Nano, 2008, 2, 441-448.	7.3	192
13	High resolution studies of small particles of gold and silver. Journal of Crystal Growth, 1981, 54, 425-432.	0.7	178
14	Thermal refugia against coral bleaching throughout the northern Red Sea. Global Change Biology, 2018, 24, e474-e484.	4.2	177
15	Atomic Structure of Symmetric Tilt Grain Boundaries in NiO. Physical Review Letters, 1987, 59, 2887-2890.	2.9	176
16	The importance of beam alignment and crystal tilt in high resolution electron microscopy. Ultramicroscopy, 1983, 11, 263-281.	0.8	173
17	Strain-Driven Alloying in Ge/Si(100) Coherent Islands. Physical Review Letters, 1999, 83, 1199-1202.	2.9	171
18	Imaging of atomic clouds outside the surfaces of gold crystals by electron microscopy. Nature, 1985, 317, 47-49.	13.7	170

#	Article	IF	CITATIONS
19	Electron Holography: Phase Imaging with Nanometer Resolution. Annual Review of Materials Research, 2007, 37, 729-767.	4.3	170
20	Synthesis, characterization, and modeling of high quality ferromagnetic Cr-doped AlN thin films. Applied Physics Letters, 2003, 82, 3047-3049.	1,5	166
21	Accurate measurements of mean inner potential of crystal wedges using digital electron holograms. Ultramicroscopy, 1993, 50, 285-299.	0.8	158
22	Formation of threading defects in GaN wurtzite films grown on nonisomorphic substrates. Applied Physics Letters, 1995, 67, 2063-2065.	1.5	158
23	Observations of grain boundary structure in submicrometer-grained Cu and Ni using high-resolution electron microscopy. Journal of Materials Research, 1998, 13, 446-450.	1.2	150
24	Evolution of Ge/Si(100) islands: Island size and temperature dependence. Journal of Applied Physics, 2000, 87, 2245-2254.	1.1	148
25	Efficient Anchoring of Silver Nanoparticles on N-Doped Carbon Nanotubes. Small, 2006, 2, 346-350.	5.2	143
26	Ultimate resolution in the electron microscope?. Materials Today, 2008, 11, 30-38.	8.3	140
27	Above 400-K robust perpendicular ferromagnetic phase in a topological insulator. Science Advances, 2017, 3, e1700307.	4.7	138
28	The Study of Heterogeneous Catalysts by High-Resolution Transmission Electron MicroscoDV. Catalysis Reviews - Science and Engineering, 1992, 34, 129-178.	5.7	136
29	Deep ultraviolet emitting AlGaN quantum wells with high internal quantum efficiency. Applied Physics Letters, 2009, 94, .	1.5	130
30	Direct observation of potential distribution across Si/Sipâ€njunctions using offâ€axis electron holography. Applied Physics Letters, 1994, 65, 2603-2605.	1,5	129
31	Endotaxial Silicide Nanowires. Physical Review Letters, 2004, 93, 256102.	2.9	119
32	Chemical Vapor Deposition Synthesis of N-, P-, and Si-Doped Single-Walled Carbon Nanotubes. ACS Nano, 2010, 4, 1696-1702.	7.3	113
33	Coral bleaching patterns are the outcome of complex biological and environmental networking. Global Change Biology, 2020, 26, 68-79.	4.2	111
34	Direct observation of the surfaces of small metal crystallites: rhodium supported on titania. Langmuir, 1988, 4, 827-830.	1.6	109
35	Power-by-the-hour: the role of technology in reshaping business strategy at Rolls-Royce. Technology Analysis and Strategic Management, 2013, 25, 987-1007.	2.0	107
36	Structural properties of InN films grown on GaAs substrates: observation of the zincblende polytpe. Journal of Crystal Growth, 1993, 127, 204-208.	0.7	104

#	Article	IF	CITATIONS
37	Reversibility of strong metal-support interactions on Rh/TiO2. Journal of Catalysis, 1989, 118, 227-237.	3.1	103
38	Spin-dependent transport ofCoâ^'SiO2granular films approaching percolation. Physical Review B, 2000, 62, 14273-14278.	1.1	100
39	Optical properties of GaN grown on ZnO by reactive molecular beam epitaxy. Applied Physics Letters, 1997, 70, 467-469.	1.5	99
40	Electron microscopy at 1-Ã resolution by entropy maximization and likelihood ranking. Nature, 1992, 355, 605-609.	13.7	97
41	Microstructure and optical properties of epitaxial GaN on ZnO (0001) grown by reactive molecular beam epitaxy. Journal of Applied Physics, 1998, 83, 983-990.	1.1	97
42	Simultaneous Enhancement of Electrical Conductivity and Thermopower of Bi ₂ Te ₃ by Multifunctionality of Native Defects. Advanced Materials, 2015, 27, 3681-3686.	11.1	97
43	The realization of atomic resolution with the electron microscope. Reports on Progress in Physics, 1997, 60, 1513-1580.	8.1	95
44	Mapping of Electrostatic Potential in Deep Submicron CMOS Devices by Electron Holography. Physical Review Letters, 2002, 89, 025502.	2.9	95
45	Sperm motility: is viscosity fundamental to progress?. Molecular Human Reproduction, 2011, 17, 539-544.	1.3	95
46	Towards quantitative electron holography of magnetic thin films using in situ magnetization reversal. Ultramicroscopy, 1998, 74, 61-73.	0.8	93
47	Vapor-liquid-solid growth of germanium nanostructures on silicon. Journal of Applied Physics, 2004, 96, 7556-7567.	1.1	92
48	The electron-beam-induced reduction of transition metal oxide surfaces to metallic lower oxides. Ultramicroscopy, 1987, 23, 299-303.	0.8	91
49	High resolution studies of small particles of gold and silver. Journal of Crystal Growth, 1981, 54, 433-438.	0.7	90
50	Direct atomic imaging of solid surfaces. Ultramicroscopy, 1985, 16, 101-113.	0.8	90
51	Magnetic interactions within patterned cobalt nanostructures using off-axis electron holography. Journal of Applied Physics, 1998, 84, 374-378.	1.1	90
52	Rapid optofluidic detection of biomarkers for traumatic brain injury via surface-enhanced Raman spectroscopy. Nature Biomedical Engineering, 2020, 4, 610-623.	11.6	87
53	Chemical vapor deposition of heteroepitaxial Si1â^'xâ^'yGexCy films on (100)Si substrates. Applied Physics Letters, 1994, 65, 2559-2561.	1.5	86
54	Characterization of structural defects in wurtzite GaN grown on 6H SiC using plasmaâ€enhanced molecular beam epitaxy. Applied Physics Letters, 1995, 67, 1830-1832.	1.5	86

#	Article	IF	CITATIONS
55	Finite size effects on the moment and ordering temperature in antiferromagnetic CoO layers. Physical Review B, 2003, 67, .	1.1	85
56	Left-Right Organizer Flow Dynamics: How Much Cilia Activity Reliably Yields Laterality?. Developmental Cell, 2014, 29, 716-728.	3.1	85
57	Interface structures in betaâ€silicon carbide thin films. Applied Physics Letters, 1987, 50, 203-205.	1.5	83
58	HREM and STEM of defects in multiplyâ€ŧwinned particles. Journal of Microscopy, 1983, 130, 249-261.	0.8	82
59	Atomic-resolution study of structural rearrangements in small platinum crystals. Ultramicroscopy, 1986, 20, 71-75.	0.8	82
60	Epitaxial lateral overgrowth of (112Â ⁻ 2) semipolar GaN on (11Â ⁻ 00) m-plane sapphire by metalorganic chemical vapor deposition. Applied Physics Letters, 2007, 90, 182109.	1.5	82
61	Enhancing Exchange Bias with Diluted Antiferromagnets. Physical Review Letters, 2006, 96, 117204.	2.9	81
62	Coral microbiome diversity reflects mass coral bleaching susceptibility during the 2016 El Niño heat wave. Ecology and Evolution, 2019, 9, 938-956.	0.8	81
63	Nanometer-scale composition measurements of Ge/Si(100) islands. Applied Physics Letters, 2003, 82, 1473-1475.	1.5	77
64	An Atomistic Branching Mechanism for Carbon Nanotubes: Sulfur as the Triggering Agent. Angewandte Chemie - International Edition, 2008, 47, 2948-2953.	7.2	76
65	Formation of a Tetrameric, Cyclooctane-like, Azidochlorogallane, [HClGaN3]4, and Related Azidogallanes. Exothermic Single-Source Precursors to GaN Nanostructures. Journal of the American Chemical Society, 1998, 120, 5233-5237.	6.6	75
66	Carrier density modulation in a germanium heterostructure by ferroelectric switching. Nature Communications, 2015, 6, 6067.	5.8	75
67	Coral microbiome composition along the northern Red Sea suggests high plasticity of bacterial and specificity of endosymbiotic dinoflagellate communities. Microbiome, 2020, 8, 8.	4.9	75
68	Quantitative analysis of one-dimensional dopant profile by electron holography. Applied Physics Letters, 2002, 80, 3213-3215.	1.5	74
69	Characterization of Al(Cr)N and Ga(Cr)N dilute magnetic semiconductors. Journal of Magnetism and Magnetic Materials, 2005, 290-291, 1395-1397.	1.0	74
70	Magnetic iron silicide nanowires on Si(110). Applied Physics Letters, 2006, 88, 113111.	1.5	73
71	Formation of metastable phases in magnesium–titanium system by high-pressure torsion and their hydrogen storage performance. Acta Materialia, 2015, 99, 150-156.	3.8	73
72	Magnetic anisotropy and microstructure in molecular beam epitaxial FePt (110)/MgO (110). Journal of Applied Physics, 1998, 84, 934-939.	1.1	72

#	Article	IF	CITATIONS
73	Procedures for focusing, stigmating and alignment in high resolution electron microscopy. Journal of Microscopy, 1983, 130, 187-201.	0.8	70
74	The determination of atomic positions in high-resolution electron micrographs. Ultramicroscopy, 1985, 18, 39-47.	0.8	70
75	Magnetic correlations in non-percolated Co–SiO2 granular films. Journal of Magnetism and Magnetic Materials, 2000, 221, 1-9.	1.0	70
76	Direct atomic imaging of solid surfaces. Surface Science, 1984, 143, 495-508.	0.8	69
77	High quality large-area CdTe(211)B on Si(211) grown by molecular beam epitaxy. Applied Physics Letters, 1997, 71, 1810-1812.	1.5	69
78	Prevention of Adrenal Crisis: Cortisol Responses to Major Stress Compared to Stress Dose Hydrocortisone Delivery. Journal of Clinical Endocrinology and Metabolism, 2020, 105, 2262-2274.	1.8	68
79	Correlation of coercivity and microstructure of thin CoFe films. Journal of Applied Physics, 2000, 88, 2058-2062.	1.1	67
80	Physics of rheologically enhanced propulsion: Different strokes in generalized Stokes. Physics of Fluids, 2013, 25, .	1.6	67
81	Direct Observation of Elastic and Plastic Deformations at Au(111) Surfaces. Physical Review Letters, 1984, 52, 656-658.	2.9	66
82	Atomic resolution electron microscopy of NiO grain boudaries. Ultramicroscopy, 1987, 22, 57-70.	0.8	66
83	Grain boundary structure in Al–Mg and Al–Mg–Sc alloys after equal-channel angular pressing. Journal of Materials Research, 2001, 16, 583-589.	1.2	66
84	Observation of vertical honeycomb structure in InAlNâ^•GaN heterostructures due to lateral phase separation. Applied Physics Letters, 2007, 90, 081917.	1.5	64
85	Plastic Deformation of BaTiO ₃ Ceramics by High-pressure Torsion and Changes in Phase Transformations, Optical and Dielectric Properties. Materials Research Letters, 2015, 3, 216-221.	4.1	64
86	Atomic-scale Chemical Imaging and Quantification of Metallic Alloy Structures by Energy-Dispersive X-ray Spectroscopy. Scientific Reports, 2014, 4, 3945.	1.6	64
87	Novel Synthetic Routes to Carbon Nitride. Chemistry of Materials, 1995, 7, 1422-1426.	3.2	61
88	Switching asymmetries in closely coupled magnetic nanostructure arrays. Applied Physics Letters, 1999, 75, 2641-2643.	1.5	61
89	Electron-beam-induced reactions at transition-metal oxide surfaces. Vacuum, 1991, 42, 301-308.	1.6	59
90	Growth and characterization of pseudomorphic single crystal zinc blende MnS. Applied Physics Letters, 1995, 67, 2690-2692.	1.5	59

#	Article	IF	CITATIONS
91	Talented suppliers? Strategic change and innovation in the UK aerospace industry. R and D Management, 2005, 35, 37-49.	3.0	58
92	Development of Aberration-Corrected Electron Microscopy. Microscopy and Microanalysis, 2008, 14, 2-15.	0.2	58
93	A homologous series of recurrent intergrowth structures of the type Bi4Am + n â^' 2Bm + nO3(m + n) + 6 formed by oxides of the aurivillius family. Journal of Solid State Chemistry, 1984, 55, 101-105.	1.4	57
94	Tunable band structure in diamond–cubic tin–germanium alloys grown on silicon substrates. Solid State Communications, 2003, 127, 355-359.	0.9	57
95	Methods for the measurement of rigid-body displacements at edge-on boundaries using high-resolution electron microscopy. Philosophical Magazine A: Physics of Condensed Matter, Structure, Defects and Mechanical Properties, 1985, 50, 375-391.	0.8	56
96	Characterization of Group III-nitride semiconductors by high-resolution electron microscopy. Journal of Crystal Growth, 1995, 152, 135-142.	0.7	56
97	Dynamic observation of defect annealing in CdTe at lattice resolution. Nature, 1982, 298, 127-131.	13.7	55
98	Dysprosium silicide nanowires on Si(110). Applied Physics Letters, 2003, 83, 5292-5294.	1.5	55
99	Effectiveness of TiN porous templates on the reduction of threading dislocations in GaN overgrowth by organometallic vapor-phase epitaxy. Applied Physics Letters, 2005, 86, 043108.	1.5	55
100	Microstructure of heteroepitaxial CdTe grown on misoriented Si(001) substrates. Applied Physics Letters, 1995, 67, 1591-1593.	1.5	54
101	Structural properties of GaN films grown on sapphire by molecular beam epitaxy. Applied Physics Letters, 1996, 68, 1141-1143.	1.5	54
102	Endotaxial silicide nanowires: A review. Thin Solid Films, 2011, 519, 8434-8440.	0.8	53
103	Origin of Magnetization Decay in Spin-Dependent Tunnel Junctions. Science, 1999, 286, 1337-1340.	6.0	52
104	Sub-250 nm room-temperature optical gain from AlGaN/AlN multiple quantum wells with strong band-structure potential fluctuations. Applied Physics Letters, 2012, 100, 061111.	1.5	52
105	The measurement of boundary displacements in metals. Ultramicroscopy, 1984, 14, 145-154.	0.8	51
106	Atomic imaging of oxide surfaces. Surface Science, 1986, 175, 673-683.	0.8	51
107	Measurement of lattice-fringe vectors from digital HREM images: experimental precision. Ultramicroscopy, 1995, 57, 409-422.	0.8	51
108	Fabrication and thermal stability of a nanocrystalline Ni–Al–Cr alloy: Comparison with pure Cu and Ni. Journal of Materials Research, 1999, 14, 4200-4207.	1.2	51

#	Article	IF	CITATIONS
109	Efficient p-type doping of GaN films by plasma-assisted molecular beam epitaxy. Applied Physics Letters, 2004, 85, 4956-4958.	1.5	51
110	The Role of Sulfur in the Synthesis of Novel Carbon Morphologies: From Covalent Yâ€Junctions to Seaâ€Urchinâ€Like Structures. Advanced Functional Materials, 2009, 19, 1193-1199.	7.8	51
111	Atomic resolution with a 600-kV electron microscope. Nature, 1979, 281, 49-51.	13.7	49
112	Non-anomalous high-resolution imaging of crystalline materials. Ultramicroscopy, 1985, 16, 19-31.	0.8	49
113	Synthesis and characterization of heteroepitaxial diamondâ€structured Ge1â^'xCx (x=1.5–5.0%) alloys using chemical vapor deposition. Applied Physics Letters, 1996, 68, 2407-2409.	1.5	49
114	Off-axis electron holography of epitaxial FePt films. Journal of Applied Physics, 1997, 82, 2461-2465.	1.1	49
115	Mapping In concentration, strain, and internal electric field in InGaN/GaN quantum well structure. Applied Physics Letters, 2004, 84, 2103-2105.	1.5	49
116	Effect of microstructure on magnetic properties and anisotropy distributions in Co/Pd thin films and nanostructures. Physical Review B, 2009, 80, .	1.1	49
117	α-1-Antitrypsin variants and the proteinase/antiproteinase imbalance in chronic obstructive pulmonary disease. American Journal of Physiology - Lung Cellular and Molecular Physiology, 2015, 308, L179-L190.	1.3	49
118	Motile curved bacteria are Pareto-optimal. Proceedings of the National Academy of Sciences of the United States of America, 2019, 116, 14440-14447.	3.3	49
119	Optimisation and applications of the Cambridge University 600 kV high resolution electron microscope. Ultramicroscopy, 1982, 9, 203-213.	0.8	48
120	The high resolution electron microscopy of stacking defects in Cu–Zn–Al shape memory alloy. Journal of Microscopy, 1983, 129, 295-306.	0.8	48
121	Magnetic tunnel junctions thermally stable to above 300 °C. Applied Physics Letters, 1999, 75, 543-545.	1.5	48
122	Annealing of CoFeB/MgO based single and double barrier magnetic tunnel junctions: Tunnel magnetoresistance, bias dependence, and output voltage. Journal of Applied Physics, 2009, 105, .	1.1	48
123	Reliability studies of AlGaN/GaN high electron mobility transistors. Semiconductor Science and Technology, 2013, 28, 074019.	1.0	48
124	Direct observation of the structure of a metallic alloy glass. Nature, 1979, 281, 465-467.	13.7	47
125	Observations of nanocrystals in thin TbFeCo films. Applied Physics Letters, 1989, 55, 919-921.	1.5	47
126	Studies of electron irradiation and annealing effects on TiO2 surfaces in ultrahigh vacuum using high-resolution electron microscopy. Surface Science, 1991, 250, 169-178.	0.8	47

#	Article	IF	CITATIONS
127	Dependence of giant magnetoresistance on Cu-layer thickness in Co/Cu multilayers: A simple dilution effect. Physical Review B, 1993, 47, 9136-9139.	1.1	47
128	Simple chemical routes to diamond-cubic germanium–tin alloys. Applied Physics Letters, 2001, 78, 3607-3609.	1.5	47
129	Impact of severe plastic deformation on microstructure and hydrogen storage of titanium-iron-manganese intermetallics. Scripta Materialia, 2016, 124, 108-111.	2.6	47
130	Epitaxial titanium silicide islands and nanowires. Surface Science, 2003, 524, 148-156.	0.8	46
131	Observation of Hole Accumulation in Ge/Si Core/Shell Nanowires Using off-Axis Electron Holography. Nano Letters, 2011, 11, 493-497.	4.5	46
132	Interaction of small and extended defects in nonstoichiometric oxides. Nature, 1984, 309, 319-321.	13.7	45
133	Electron microscopy study of Ni/Ni3Al diffusion-couple interface—l. Microstructural observation and microchemical analysis. Acta Metallurgica Et Materialia, 1994, 42, 3381-3387.	1.9	45
134	Quantitative phase imaging of nanoscale electrostatic and magnetic fields using off-axis electron holography. Ultramicroscopy, 2010, 110, 375-382.	0.8	45
135	Atomic and electronic structure of the ferroelectric BaTiO3/Ge(001) interface. Applied Physics Letters, 2014, 104, .	1.5	45
136	Evaluation of antimony segregation in InAs/InAs1â^'xSbx type-II superlattices grown by molecular beam epitaxy. Journal of Applied Physics, 2016, 119, .	1.1	45
137	Oriented Growth of Single-Crystal Ni Nanowires onto Amorphous SiO ₂ . Nano Letters, 2010, 10, 5070-5075.	4.5	44
138	Epitaxial strontium titanate films grown by atomic layer deposition on SrTiO3-buffered Si(001) substrates. Journal of Vacuum Science and Technology A: Vacuum, Surfaces and Films, 2013, 31, .	0.9	44
139	Low-threshold continuous-wave operation of quantum-cascade lasers grown by metalorganic vapor phase epitaxy. Applied Physics Letters, 2004, 85, 5842-5844.	1.5	43
140	Defect characterization for epitaxial HgCdTe alloys by electron microscopy. Journal of Crystal Growth, 2004, 265, 224-234.	0.7	43
141	Atomic layer deposition of crystalline SrHfO3 directly on Ge (001) for high- <i>k</i> dielectric applications. Journal of Applied Physics, 2015, 117, .	1.1	43
142	Applications of electron holography to the study of interfaces. Ultramicroscopy, 1993, 50, 301-311.	0.8	42
143	SnGe superstructure materials for Si-based infrared optoelectronics. Applied Physics Letters, 2003, 83, 3489-3491.	1.5	42
144	Reverse Leakage Analysis for As-Grown and Regrown Vertical GaN-on-GaN Schottky Barrier Diodes. IEEE Journal of the Electron Devices Society, 2020, 8, 74-83.	1.2	42

#	Article	IF	CITATIONS
145	Atom hopping on small gold particles imaged by high-resolution electron microscopy. Die Naturwissenschaften, 1985, 72, 539-541.	0.6	41
146	A Joint Structural Characterization of Colloidal Platinum by EXAFS and High-Resolution Electron Microscopy. Angewandte Chemie International Edition in English, 1989, 28, 590-593.	4.4	41
147	Spin-dependent tunneling in discontinuous Co–SiO2 magnetic tunnel junctions. Applied Physics Letters, 1998, 73, 535-537.	1.5	41
148	Influence of interface alloying on the magnetic properties of Co/Pd multilayers. Applied Physics Letters, 2003, 83, 5259-5261.	1.5	41
149	Hollow metallic microspheres produced by spark erosion. Applied Physics Letters, 2004, 85, 940-942.	1.5	41
150	The role of Cr substitution on the ferromagnetic properties of Ga1â^'xCrxN. Applied Physics Letters, 2005, 86, 012504.	1.5	41
151	Modelling the fluid mechanics of cilia and flagella in reproduction and development. European Physical Journal E, 2012, 35, 111.	0.7	41
152	Real-Time Atomic-Resolution Imaging of Polymorphic Changes in Ruthenium Clusters. Angewandte Chemie International Edition in English, 1988, 27, 555-558.	4.4	40
153	Growth and characterization of CdTe/Si heterostructures — effect of substrate orientation. Materials Science and Engineering B: Solid-State Materials for Advanced Technology, 2000, 77, 93-100.	1.7	40
154	Decorating carbon nanotubes with nanostructured nickel particles via chemical methods. Chemical Physics Letters, 2006, 431, 104-109.	1.2	40
155	Quenched magnetic moment in Mn-doped amorphous Si films. Physical Review B, 2008, 77, .	1.1	40
156	A Chemical Route to Monolithic Integration of Crystalline Oxides on Semiconductors. Advanced Materials Interfaces, 2014, 1, 1400081.	1.9	40
157	Large positive linear magnetoresistance in the two-dimensional t 2g electron gas at the EuO/SrTiO3 interface. Scientific Reports, 2018, 8, 7721.	1.6	40
158	Direct lattice imaging of small metal particles. Philosophical Magazine A: Physics of Condensed Matter, Structure, Defects and Mechanical Properties, 1981, 44, 735-740.	0.8	39
159	"Metallisation―of oxide surfaces observed by in situ high-resolution electron microscopy. Ultramicroscopy, 1985, 17, 387-391.	0.8	39
160	The oxidation of small rhodium metal particles. Ultramicroscopy, 1989, 31, 132-137.	0.8	38
161	Novel chemical routes to siliconâ€germaniumâ€carbon materials. Applied Physics Letters, 1994, 65, 2960-2962.	1.5	38
162	Influence of 6H–SiC(0001) substrate surface morphology on the growth of AlN epitaxial layers. Applied Physics Letters, 1999, 74, 985-987.	1.5	38

#	Article	IF	CITATIONS
163	Molecular beam epitaxy of InAlNâ^•GaN heterostructures for high electron mobility transistors. Journal of Vacuum Science & Technology an Official Journal of the American Vacuum Society B, Microelectronics Processing and Phenomena, 2005, 23, 1204.	1.6	38
164	Complex and incommensurate ordering in Al0.72Ga0.28N thin films grown by plasma-assisted molecular beam epitaxy. Applied Physics Letters, 2006, 88, 181915.	1.5	38
165	Electric-Field-Driven Degradation in off-State Step-Stressed AlGaN/GaN High-Electron Mobility Transistors. IEEE Transactions on Device and Materials Reliability, 2011, 11, 187-193.	1.5	38
166	Observations of silicon carbide by high resolution transmission electron microscopy. Journal of Microscopy, 1978, 114, 1-18.	0.8	37
167	A systematic analysis of HREM imaging of sphalerite semiconductors. Ultramicroscopy, 1989, 27, 131-150.	0.8	37
168	Epitaxial relationships in electron-stimulated desorption processes at transition metal oxide surfaces. Surface Science, 1989, 221, 214-232.	0.8	37
169	Development of a low-temperature GaN chemical vapor deposition process based on a single molecular source H2GaN3. Applied Physics Letters, 1999, 74, 883-885.	1.5	37
170	Intersubband absorption in AlNâ^•GaNâ^•AlGaN coupled quantum wells. Applied Physics Letters, 2007, 91, 141104.	1.5	37
171	Quasi-two-dimensional electron gas at the epitaxial alumina/SrTiO3 interface: Control of oxygen vacancies. Journal of Applied Physics, 2015, 117, .	1.1	37
172	Unraveling Hydrophobic Interactions at the Molecular Scale Using Force Spectroscopy and Molecular Dynamics Simulations. ACS Nano, 2017, 11, 2586-2597.	7.3	37
173	Determination of mean inner potential of germanium using off-axis electron holography. Acta Crystallographica Section A: Foundations and Advances, 1999, 55, 652-658.	0.3	36
174	Structure and orientation of epitaxial titanium silicide nanowires determined by electron microdiffraction. Journal of Applied Physics, 2003, 93, 5670-5674.	1.1	36
175	Defects at the surface of \hat{l}^2 -Ga2O3 produced by Ar plasma exposure. APL Materials, 2019, 7, .	2.2	36
176	A theoretical analysis of HREM imaging for ã€^110〉 tetrahedral semiconductors. Ultramicroscopy, 1989, 27, 19-34.	0.8	35
177	Dependence of giant magnetoresistance on grain size in Co/Cu multilayers. Physical Review B, 1994, 50, 4232-4235.	1.1	35
178	Long wavelength (1.3 and 1.5 μm) photoluminescence from InGaAs/GaPAsSb quantum wells grown on GaAs. Applied Physics Letters, 1999, 75, 1267-1269.	1.5	35
179	Defect annihilation in AlN thin films by ultrahigh temperature processing. Applied Physics Letters, 2000, 76, 1839-1841.	1.5	35
180	Semiconductor dopant profiling by off-axis electron holography. Ultramicroscopy, 2003, 94, 149-161.	0.8	35

#	Article	IF	CITATIONS
181	Nanosynthesis Routes to New Tetrahedral Crystalline Solids: Silicon-like Si ₃ AlP. Journal of the American Chemical Society, 2011, 133, 16212-16218.	6.6	35
182	Characterization of Bi2Te3 and Bi2Se3 topological insulators grown by MBE on (001) GaAs substrates. Journal of Vacuum Science and Technology B:Nanotechnology and Microelectronics, 2012, 30, .	0.6	35
183	Magnetically soft, high-moment, high-resistivity thin films using discontinuous metal/native oxide multilayers. Applied Physics Letters, 2001, 79, 224-226.	1.5	34
184	Microstructural evolution of Ge/Si(100) nanoscale islands. Journal of Crystal Growth, 2003, 259, 232-244.	0.7	34
185	Magnetic domain configurations in spark-eroded ferromagnetic shape memory Ni-Mn-Ga particles. Applied Physics Letters, 2005, 86, 192503.	1.5	34
186	Understanding ion-milling damage in Hg1â^'xCdxTe epilayers. Journal of Vacuum Science and Technology A: Vacuum, Surfaces and Films, 2006, 24, 995-1000.	0.9	34
187	Optically pumped intersubband emission of short-wave infrared radiation with GaN/AlN quantum wells. Applied Physics Letters, 2009, 94, 081120.	1.5	34
188	Direct Mapping of Charge Distribution during Lithiation of Ge Nanowires Using Off-Axis Electron Holography. Nano Letters, 2016, 16, 3748-3753.	4.5	34
189	Development of AlGaN-based graded-index-separate-confinement-heterostructure deep UV emitters by molecular beam epitaxy. Journal of Vacuum Science and Technology B:Nanotechnology and Microelectronics, 2013, 31, .	0.6	33
190	Direct imaging of surface reconstructions on CdTe by high-resolution electron microscopy. Physical Review Letters, 1987, 59, 2177-2179.	2.9	32
191	Profile imaging of surfaces and surface reactions. Ultramicroscopy, 1989, 29, 123-134.	0.8	32
192	Growth of high quality CdTe on Si substrates by molecular beam epitaxy. Journal of Electronic Materials, 1996, 25, 1402-1405.	1.0	32
193	Structural characterization of thin film ferromagnetic tunnel junctions. Journal of Applied Physics, 1998, 83, 5154-5158.	1.1	32
194	Homoepitaxial growth of (0001)- and -oriented ZnO thin films via metalorganic vapor-phase epitaxy and their characterization. Journal of Crystal Growth, 2004, 265, 390-398.	0.7	32
195	Polarization field mapping of Al0.85In0.15N/AlN/GaN heterostructure. Applied Physics Letters, 2009, 94, ·	1.5	32
196	High-Performance AlN/GaN HEMTs on Sapphire Substrate With an Oxidized Gate Insulator. IEEE Electron Device Letters, 2011, 32, 1677-1679.	2.2	32
197	Fabrication of nanograined silicon by high-pressure torsion. Journal of Materials Science, 2014, 49, 6565-6569.	1.7	32
198	HREM, STEM, REM, SEM — and STM. Surface Science, 1987, 181, 235-249.	0.8	31

#	Article	IF	CITATIONS
199	The effect of carbon on strain relaxation and phase formation in the Ti/Si1â^'xâ^'yGexCy/Si contact system. Applied Physics Letters, 1996, 69, 64-66.	1.5	31
200	Molecular Synthesis of High-Performance Near-IR Photodetectors with Independently Tunable Structural and Optical Properties Based on Si–Ge–Sn. Journal of the American Chemical Society, 2012, 134, 20756-20767.	6.6	31
201	Characterization of Nanomaterials Using Transmission Electron Microscopy. RSC Nanoscience and Nanotechnology, 2015, , 1-29.	0.2	31
202	Investigations of the structure of amorphous and partially crystalline metallic alloys by high resolution electron microscopy. Journal of Microscopy, 1980, 119, 63-72.	0.8	30
203	Ultra-high-resolution electron microscopy of amorphous materials at 120 kV. The Philosophical Magazine: Physics of Condensed Matter B, Statistical Mechanics, Electronic, Optical and Magnetic Properties, 1981, 43, 907-923.	0.6	30
204	The hollandite-related structure of Ba2Ti9O20. Journal of Solid State Chemistry, 1983, 47, 151-163.	1.4	30
205	Recent improvements to the Cambridge University 600 kV High Resolution Electron Microscope. Journal of Microscopy, 1983, 130, 127-136.	0.8	30
206	Radiation damage and structural studies: Halogenated phthalocyanines. Ultramicroscopy, 1986, 19, 279-297.	0.8	30
207	Observation of exit surface sputtering in TiO2 using biased secondary electron imaging. Surface Science, 1990, 237, 232-240.	0.8	30
208	Direct imaging of CdTe(001) surface reconstructions by high-resolution electron microscopy. Surface Science, 1991, 254, 119-124.	0.8	30
209	Evolution of grain boundary structure in submicrometer-grained Al-Mg alloy. Materials Characterization, 1996, 37, 285-294.	1.9	30
210	Far-infrared detector based on HgTe/HgCdTe superlattices. Journal of Electronic Materials, 2003, 32, 608-614.	1.0	30
211	Polarizationâ€Induced Charge Distribution at Homogeneous Zincblende/Wurtzite Heterostructural Junctions in ZnSe Nanobelts. Advanced Materials, 2012, 24, 1328-1332.	11.1	30
212	Quasi-two-dimensional electron gas at the interface of γ-Al2O3/SrTiO3 heterostructures grown by atomic layer deposition. Journal of Applied Physics, 2015, 118, .	1.1	30
213	Mercury cadmium telluride/tellurium intergrowths in HgCdTe epilayers grown by molecular-beam epitaxy. Applied Physics Letters, 2003, 82, 2275-2277.	1.5	29
214	Atomic-scale imaging of asymmetric Lomer dislocation cores at the Ge/Si(001) heterointerface. Applied Physics Letters, 2004, 84, 2530-2532.	1.5	29
215	Distinct local electronic structure and magnetism for Mn in amorphous Si and Ge. Physical Review B, 2010, 82, .	1.1	29
216	Strain-balanced InAs/InAs1â^'xSbx type-II superlattices grown by molecular beam epitaxy on GaSb substrates. Journal of Vacuum Science and Technology B:Nanotechnology and Microelectronics, 2012, 30, .	0.6	29

#	Article	IF	CITATIONS
217	Green innovation and the development of sustainable communities. International Journal of Entrepreneurship and Innovation, 2018, 19, 21-32.	1.4	29
218	Damage Recovery and Dopant Diffusion in Si and Sn Ion Implanted β-Ga ₂ O ₃ . ECS Journal of Solid State Science and Technology, 2019, 8, Q3133-Q3139.	0.9	29
219	Elastic strain at the solid-solid interface in intergrowth structures : A novel example of partial structure refinement by HREM. Materials Research Bulletin, 1984, 19, 1403-1409.	2.7	28
220	Low temperature inorganic chemical vapor deposition of heteroepitaxial GaN. Applied Physics Letters, 1996, 69, 203-205.	1.5	28
221	Synthesis and Atomic and Electronic Structure of New Siâ^'Geâ^'C Alloys and Compounds. Chemistry of Materials, 1998, 10, 2935-2949.	3.2	28
222	Polarity determination and atomic arrangements at a GaN/SiC interface using high-resolution image matching. Applied Physics Letters, 2000, 76, 822-824.	1.5	28
223	Evolution of Ge/Si(100) island morphology at high temperature. Applied Physics Letters, 2002, 80, 3623-3625.	1.5	28
224	New Magnetic Order in Buried Native Iron Oxide Layers. Physical Review Letters, 2003, 91, 267201.	2.9	28
225	Growth of Illâ€nitride quantum dots and their applications to blueâ€green LEDs. Physica Status Solidi (A) Applications and Materials Science, 2008, 205, 2560-2565.	0.8	28
226	Ti/Al/Ni/Au Ohmic contacts for AlInN/AlN/GaN-based heterojunction field-effect transistors. Journal of Applied Physics, 2010, 107, .	1.1	28
227	Negative Tunneling Magnetoresistance by Canted Magnetization in <mml:math xmlns:mml="http://www.w3.org/1998/Math/MathML" display="inline"><mml:mi>MgO</mml:mi><mml:mo>/</mml:mo><mml:mi>NiO</mml:mi>Tunnel Barriers. Physical Review Letters, 2011, 106, 167201.</mml:math 	2.9	28
228	Measurement and effects of polarization fields on one-monolayer-thick InN/GaN multiple quantum wells. Physical Review B, 2013, 88, .	1.1	28
229	Critical issues for homoepitaxial GaN growth by molecular beam epitaxy on hydride vapor-phase epitaxy-grown GaN substrates. Journal of Crystal Growth, 2016, 456, 121-132.	0.7	28
230	Microstructural and optical characterization of CdTe(211)B/ZnTe/Si(211) grown by molecular beam epitaxy. Journal of Electronic Materials, 1998, 27, 1047-1052.	1.0	27
231	Interlayer coupling within individual submicron magnetic elements. Journal of Applied Physics, 2000, 87, 7400-7404.	1.1	27
232	The formation of ordered, ultrathin SiO2/Si(100) interfaces grown on (1×1) Si(100). Materials Science and Engineering B: Solid-State Materials for Advanced Technology, 2001, 87, 303-316.	1.7	27
233	Formation mechanism of crater defects on HgCdTe/CdZnTe (211) B epilayers grown by molecular beam epitaxy. Applied Physics Letters, 2003, 83, 4785-4787.	1.5	27
234	Sign of tunneling magnetoresistance in CrO2-based magnetic tunnel junctions. Applied Physics Letters, 2007, 91, 252506.	1.5	27

#	Article	IF	CITATIONS
235	Determination of the Inelastic Mean-Free-Path and Mean Inner Potential for AlAs and GaAs Using Off-Axis Electron Holography and Convergent Beam Electron Diffraction. Microscopy and Microanalysis, 2007, 13, 329-335.	0.2	27
236	Epitaxy of polar semiconductor Co3O4 (110): Growth, structure, and characterization. Journal of Applied Physics, 2014, 115, .	1.1	27
237	Determination of Polarizationâ€Fields Across Polytype Interfaces in InAs Nanopillars. Advanced Materials, 2014, 26, 1052-1057.	11.1	27
238	A roadmap to integrating resilience into the practice of coral reef restoration. Global Change Biology, 2022, 28, 4751-4764.	4.2	27
239	Atomic imaging of oxide surfaces. Surface Science, 1986, 175, 684-692.	0.8	26
240	Atomic imaging of surfaces by electron microscopy. Surface Science, 1986, 178, 462-474.	0.8	26
241	A systematic analysis of HREM imaging of elemental semiconductors. Ultramicroscopy, 1989, 27, 35-51.	0.8	26
242	Electron microscopy of surface-crater defects on HgCdTe/CdZnTe(211)B epilayers grown by molecular-beam epitaxy. Journal of Electronic Materials, 2003, 32, 703-709.	1.0	26
243	Epitaxial DySi2 nanowire formation on stepped Si(111). Applied Physics Letters, 2005, 86, 143110.	1.5	26
244	Phase transformation in FeSi2 nanowires. Journal of Crystal Growth, 2006, 295, 166-171.	0.7	26
245	Effects of vortex chirality and shape anisotropy on magnetization reversal of Co nanorings (invited). Journal of Applied Physics, 2010, 107, .	1.1	26
246	Oxygen vacancy-mediated room-temperature ferromagnetism in insulating cobalt-substituted SrTiO <mml:math <br="" xmlns:mml="http://www.w3.org/1998/Math/MathML">display="inline"><mml:msub><mml:mrow></mml:mrow><mml:mn>3</mml:mn></mml:msub></mml:math> epitaxially integrated with silicon. Physical Review B, 2013, 87, .	1.1	26
247	Performance and reproducibility enhancement of HgCdTe molecular beam epitaxy growth on CdZnTe substrates using interfacial HgTeâ^•CdTe superlattice layers. Applied Physics Letters, 2005, 86, 131924.	1.5	25
248	Evidence of modified ferromagnetism at a buried Permalloy/CoO interface at room temperature. Physical Review B, 2007, 75, .	1.1	25
249	Effect of source field plate on the characteristics of off-state, step-stressed AlGaN/GaN high electron mobility transistors. Journal of Vacuum Science and Technology B:Nanotechnology and Microelectronics, 2011, 29, .	0.6	25
250	Electroluminescence and Transmission Electron Microscopy Characterization of Reverse-Biased AlGaN/GaN Devices. IEEE Transactions on Device and Materials Reliability, 2013, 13, 126-135.	1.5	25
251	Molecular beam epitaxy using bismuth as a constituent in InAs and a surfactant in InAs/InAsSb superlattices. Journal of Vacuum Science and Technology B:Nanotechnology and Microelectronics, 2014, 32, .	0.6	25
252	The sound of recovery: Coral reef restoration success is detectable in the soundscape. Journal of Applied Ecology, 2022, 59, 742-756.	1.9	25

#	Article	IF	CITATIONS
253	High resolution imaging of amorphous materials. Nature, 1979, 281, 54-55.	13.7	24
254	High-resolution images of bent crystals having rutile-type structures: Tin dioxide. Philosophical Magazine A: Physics of Condensed Matter, Structure, Defects and Mechanical Properties, 1982, 45, 771-789.	0.8	24
255	Point, linear and extended defect structures in nonstoichiometric rutile. Radiation Effects, 1983, 74, 253-265.	0.4	24
256	The observation of in situ and ex situ oxidation processes for ZnTe surfaces by high-resolution electron microscopy. Physica Status Solidi A, 1988, 107, 681-691.	1.7	24
257	Growth of heteroepitaxial Si1â^'xâ^'yGexCy alloys on silicon using novel deposition chemistry. Applied Physics Letters, 1995, 67, 1247-1249.	1.5	24
258	Growth and characterization of Si1â^'xMnx alloys on Si(100). Journal of Applied Physics, 2005, 98, 033512.	1.1	24
259	InGaN/GaN multiple-quantum-well light-emitting diodes grown on Si(111) substrates with ZrB2(0001) buffer layers. Journal of Applied Physics, 2012, 111, 033107.	1.1	24
260	Surface preparation of freestanding GaN substrates for homoepitaxial GaN growth by rf-plasma MBE. Journal of Vacuum Science and Technology B:Nanotechnology and Microelectronics, 2017, 35, .	0.6	24
261	Self-assembled Bismuth Selenide (Bi2Se3) quantum dots grown by molecular beam epitaxy. Scientific Reports, 2019, 9, 3370.	1.6	24
262	Aperture contrast in thick amorphous specimens using scanning transmission electron microscopy. Ultramicroscopy, 1975, 1, 127-136.	0.8	23
263	Electron irradiation effects in (Cs,Ba)-hollandites. Journal of Solid State Chemistry, 1987, 69, 343-354.	1.4	23
264	CdTe(111)B grown on Si(111) by molecular beam epitaxy. Applied Physics Letters, 1999, 74, 2346-2348.	1.5	23
265	Faulted surface layers in dysprosium silicide nanowires. Physical Review B, 2004, 70, .	1.1	23
266	Effect of Alâ^•N ratio during nucleation layer growth on Hall mobility and buffer leakage of molecular-beam epitaxy grown AlGaNâ^•GaN heterostructures. Applied Physics Letters, 2004, 85, 3786-3788.	1.5	23
267	Ultrathin-barrier AlN/GaN heterostructures grown by rf plasma-assisted molecular beam epitaxy on freestanding GaN substrates. Journal of Crystal Growth, 2013, 380, 14-17.	0.7	23
268	Guided VLS Growth of Epitaxial Lateral Si Nanowires. Nano Letters, 2013, 13, 3878-3883.	4.5	23
269	Clyph-Based Video Visualization for Semen Analysis. IEEE Transactions on Visualization and Computer Graphics, 2015, 21, 980-993.	2.9	23
270	High-resolution transmission electron microscopy analysis of nanograined germanium produced by high-pressure torsion. Materials Characterization, 2017, 132, 132-138.	1.9	23

#	Article	IF	CITATIONS
271	Direct atomic imaging of solid surfaces. Surface Science, 1985, 157, L367-L372.	0.8	22
272	<i>In situ</i> oxidation processes for In III-V compound semiconductors studied by high-resolution electron microscopy. Philosophical Magazine A: Physics of Condensed Matter, Structure, Defects and Mechanical Properties, 1986, 54, 837-850.	0.8	22
273	Dynamic edge and surface processes in terbium oxide. Ultramicroscopy, 1987, 22, 71-79.	0.8	22
274	Surface facetting and polarity of alumina. Ultramicroscopy, 1987, 23, 223-227.	0.8	22
275	Enhanced internal quantum efficiency and light extraction efficiency from textured GaNâ^•AlGaN quantum wells grown by molecular beam epitaxy. Journal of Applied Physics, 2006, 99, 064904.	1.1	22
276	Sequential tunneling transport characteristics of GaN/AlGaN coupled-quantum-well structures. Journal of Applied Physics, 2010, 108, 103704.	1.1	22
277	Symmetry breaking cilia-driven flow in the zebrafish embryo. Journal of Fluid Mechanics, 2012, 705, 26-45.	1.4	22
278	Effect of SrTiO ₃ oxygen vacancies on the conductivity of LaTiO ₃ /SrTiO ₃ heterostructures. Journal of Applied Physics, 2018, 124, 185303.	1.1	22
279	Quantitative measurement of nanoscale electrostatic potentials and charges using off-axis electron holography: Developments and opportunities. Ultramicroscopy, 2019, 203, 105-118.	0.8	22
280	A systematic analysis of HREM imaging of Wurtzite semiconductors. Ultramicroscopy, 1989, 27, 117-130.	0.8	21
281	Effect of ammonia flow rate on impurity incorporation and material properties of Si-doped GaN epitaxial films grown by reactive molecular beam epitaxy. Journal of Applied Physics, 1998, 84, 6680-6685.	1.1	21
282	Electrical, microstructural, and thermal stability characteristics of Ta/Ti/Ni/Au contacts to n-GaN. Journal of Applied Physics, 2004, 95, 1516-1524.	1.1	21
283	Microstructural characterization of Ni-Mn-Ga ferromagnetic shape memory alloy powders. Journal of Applied Physics, 2004, 95, 6954-6956.	1.1	21
284	Internally shunted Josephson junctions with barriers tuned near the metal–insulator transition for RSFQ logic applications. Superconductor Science and Technology, 2006, 19, 719-731.	1.8	21
285	Real-time x-ray studies of gallium nitride nanodot formation by droplet heteroepitaxy. Journal of Applied Physics, 2007, 102, .	1.1	21
286	Microwave performance and structural characterization of MBE-grown AlGaN/GaN HEMTs on low dislocation density GaN substrates. Journal of Crystal Growth, 2007, 305, 340-345.	0.7	21
287	Structural characterization of non-polar (1120) and semi-polar (1126) GaN films grown on r-plane sapphire. Journal of Crystal Growth, 2008, 310, 2981-2986.	0.7	21
288	Progress and perspectives for atomic-resolution electron microscopy. Ultramicroscopy, 2008, 108, 159-166.	0.8	21

#	Article	IF	CITATIONS
289	Microstructural characterization of thick ZnTe epilayers grown on GaSb, InAs, InP and GaAs (100) substrates. Journal of Crystal Growth, 2011, 330, 30-34.	0.7	21
290	Reinventing artisanal knowledge and practice: a critical review of innovation in a craft-based industry. Prometheus, 2013, 31, .	0.2	21
291	Effect of proton irradiation on AlGaN/GaN high electron mobility transistor off-state drain breakdown voltage. Applied Physics Letters, 2014, 104, .	1.5	21
292	Improvisation and Entrepreneurial Bricolage versus Rationalisation: A case-based analysis of contrasting responses to economic instability in the UK brass musical instruments industry. Journal of General Management, 2014, 40, 53-78.	0.8	21
293	Meshfree and efficient modeling of swimming cells. Physical Review Fluids, 2018, 3, .	1.0	21
294	On the growth of small crystals of Cd, Zn, Pt and Rh during electron microscope observations. Journal of Crystal Growth, 1987, 80, 218-224.	0.7	20
295	Growth of AlN and GaN on 6H–SiC(0001) using a helium supersonic beam seeded with ammonia. Applied Physics Letters, 1997, 71, 1365-1367.	1.5	20
296	Off-axis electron holography of exchange-biased CoFe/FeMn patterned nanostructures. Journal of Applied Physics, 2001, 90, 2899-2902.	1.1	20
297	Study of in situ magnetization reversal processes for nanoscale Co rings using off-axis electron holography. Journal of Applied Physics, 2005, 97, 054305.	1.1	20
298	Dislocation reduction in GaN grown on porous TiN networks by metal-organic vapor-phase epitaxy. Journal of Applied Physics, 2006, 99, 033518.	1.1	20
299	Epitaxial lateral overgrowth of non-polar GaN(11Ì,,00) on Si(112) patterned substrates by MOCVD. Journal of Crystal Growth, 2011, 314, 129-135.	0.7	20
300	Investigation of MBE-grown InAs1â`'Bi alloys and Bi-mediated type-II superlattices by transmission electron microscopy. Journal of Crystal Growth, 2015, 425, 250-254.	0.7	20
301	Band offsets of epitaxial cubic boron nitride deposited on polycrystalline diamond via plasma-enhanced chemical vapor deposition. Applied Physics Letters, 2017, 111, 171604.	1.5	20
302	Institutions, place leadership and public entrepreneurship: Reinterpreting the economic development of Nottingham. Local Economy, 2017, 32, 374-392.	0.8	20
303	Investigations of the tin-antimony-oxygen system by high-resolution electron microscopy. Journal of Solid State Chemistry, 1982, 44, 326-336.	1.4	19
304	Supercell ordering in a hollandite-type phase: Potassium magnesium antimony oxide. Journal of Solid State Chemistry, 1983, 46, 373-381.	1.4	19
305	Characterization of Siâ€implanted and electronâ€beamâ€annealed siliconâ€onâ€sapphire using highâ€resolution electron microscopy. Journal of Applied Physics, 1984, 56, 2207-2212.	1.1	19
306	Emergence of small defect contrast within HREM images of nonstoichiometric rutile. Ultramicroscopy, 1984, 13, 191-204.	0.8	19

#	Article	IF	CITATIONS
307	Microstructural characterization of Co/Cu multilayers. Journal of Magnetism and Magnetic Materials, 1994, 129, 415-422.	1.0	19
308	Increasing the exchange-bias field of Ni0.5Co0.5O films by microstructural control. Applied Physics Letters, 1999, 74, 1314-1316.	1.5	19
309	Introduction: An International Workshop in Honor of Regents' Professor John Maxwell Cowley on the Occasion of His 80th Birthday. Microscopy and Microanalysis, 2004, 10, 1-3.	0.2	19
310	Improve molecular beam epitaxy growth of HgCdTe on CdZnTe (211)B substrates using interfacial layers of HgTeâ^•CdTe superlattices. Journal of Applied Physics, 2006, 100, 114316.	1.1	19
311	GaN quantum dot superlattices grown by molecular beam epitaxy at high temperature. Journal of Applied Physics, 2007, 102, 073517.	1.1	19
312	Simulation of polarization charge on AlGaN/GaN high electron mobility transistors: Comparison to electron holography. Journal of Applied Physics, 2010, 107, 054516.	1.1	19
313	Growth of epitaxial oxides on silicon using atomic layer deposition: Crystallization and annealing of TiO2 on SrTiO3-buffered Si(001). Journal of Vacuum Science and Technology B:Nanotechnology and Microelectronics, 2012, 30, 04E111.	0.6	19
314	Mapping electrostatic profiles across axial <i>p-n</i> junctions in Si nanowires using off-axis electron holography. Applied Physics Letters, 2013, 103, .	1.5	19
315	High-resolution transmission electron microscopy analysis of bulk nanograined silicon processed by high-pressure torsion. Materials Characterization, 2017, 129, 163-168.	1.9	19
316	Dissociated 60° dislocations in CdTe studied by high-resolution electron microscopy. The Philosophical Magazine: Physics of Condensed Matter B, Statistical Mechanics, Electronic, Optical and Magnetic Properties, 1990, 62, 435-450.	0.6	18
317	Inversion of surface composition and evolution of nanostructure in Cu/Co nanocrystals. Applied Physics Letters, 1999, 74, 3161-3163.	1.5	18
318	Beneficial effects of annealing on amorphous Nb–Si thin-film thermometers. Applied Physics Letters, 2005, 87, 221901.	1.5	18
319	Structural and electrical properties of Pb(Zr,Ti)O3 films grown by molecular beam epitaxy. Applied Physics Letters, 2007, 91, .	1.5	18
320	Production and detailed characterization of bean husk-based carbon: Efficient cadmium (II) removal from aqueous solutions. Water Research, 2008, 42, 3473-3479.	5.3	18
321	Large electro-optic effect in single-crystal Pb(Zr,Ti)O3 (001) measured by spectroscopic ellipsometry. Journal of Applied Physics, 2008, 104, 093103.	1.1	18
322	Observation of asymmetrical pinning of domain walls in notched Permalloy nanowires using electron holography. Applied Physics Letters, 2009, 95, 182507.	1.5	18
323	Proton irradiation effects on AlN/GaN high electron mobility transistors. Journal of Vacuum Science and Technology B:Nanotechnology and Microelectronics, 2010, 28, L47-L51.	0.6	18
324	Switching Behavior and Forward Bias Degradation of 700V, 0.2A, β-Ga ₂ O ₃ Vertical Geometry Rectifiers. ECS Journal of Solid State Science and Technology, 2019, 8, Q3028-Q3033.	0.9	18

#	Article	IF	CITATIONS
325	⁶⁰ Co Gamma Ray Damage in Homoepitaxial β-Ga ₂ O ₃ Schottky Rectifiers. ECS Journal of Solid State Science and Technology, 2019, 8, Q3041-Q3045.	0.9	18
326	Molecular detail in electron micrographs of quaterrylene C40H20. Nature, 1981, 291, 481-482.	13.7	17
327	Progress towards quantitative high-resolution electron microscopy. Ultramicroscopy, 1993, 52, 591-601.	0.8	17
328	Growth and characterization of thin Si80C20 films based upon Si4C building blocks. Applied Physics Letters, 1998, 72, 930-932.	1.5	17
329	Morphological control and structural characteristics of crystalline Ge–C systems: Carbide nanorods, quantum dots, and epitaxial heterostructures. Applied Physics Letters, 1999, 74, 958-960.	1.5	17
330	Switching mechanisms and remanent states for nanoscale slotted Co circular elements studied by electron holography. Physical Review B, 2006, 73, .	1.1	17
331	One-step production of optimized Fe–Ga particles by spark erosion. Applied Physics Letters, 2006, 89, 142506.	1.5	17
332	Viscosity of aqueous DNA solutions determined using dynamic light scattering. Analyst, The, 2011, 136, 4159.	1.7	17
333	High resolution electron microscopic study of tin dioxide crystals. Journal of Solid State Chemistry, 1983, 50, 51-69.	1.4	16
334	The application of high resolution electron microscopy to the study of oxidation. Journal of Microscopy, 1983, 130, 137-146.	0.8	16
335	Approaching atomic-resolution electron microscopy. Ultramicroscopy, 1985, 18, 63-75.	0.8	16
336	Surface polarity determination in ã€^110〉-orientated compound semiconductors high-resolution electron microscopy. Philosophical Magazine Letters, 1989, 59, 69-75.	0.5	16
337	Characterization of surface structure in heterogeneous catalysts by high-resolution transmission electron microscopy. Ultramicroscopy, 1990, 34, 47-53.	0.8	16
338	Comparative study of supported catalyst particles by electron microscopy methods. Ultramicroscopy, 1993, 52, 282-288.	0.8	16
339	on GaAs grown by molecular beam epitaxy. Journal of Crystal Growth, 1996, 159, 94-98.	0.7	16
340	Low-temperature growth of SiCAlN films of high hardness on Si(111) substrates. Applied Physics Letters, 2001, 79, 2880-2882.	1.5	16
341	Morphological and optical properties of Si nanostructures imbedded in SiO2 and Si3N4 films grown by single source chemical vapor deposition. Journal of Applied Physics, 2002, 92, 7475-7480.	1.1	16
342	In situ studies of the role of excess Ga on the growth morphology of thin GaN layers. Surface Science, 2002, 496, 160-178.	0.8	16

#	Article	IF	CITATIONS
343	Reconstruction technique for off-axis electron holography using coarse fringes. Ultramicroscopy, 2006, 106, 486-491.	0.8	16
344	Microstructure of relaxed InN quantum dots grown on GaN buffer layers by molecular-beam epitaxy. Applied Physics Letters, 2006, 88, 231906.	1.5	16
345	Financial bootstrapping and social capital: how technology-based start-ups fund innovation. International Journal of Entrepreneurship and Innovation Management, 2009, 10, 199.	0.1	16
346	Synthesis and Materials Properties of Sn/P-Doped Ge on Si(100): Photoluminescence and Prototype Devices. Chemistry of Materials, 2011, 23, 4480-4486.	3.2	16
347	Measurement of electric field across individual wurtzite GaN quantum dots using electron holography. Applied Physics Letters, 2011, 99, .	1.5	16
348	Molecular Dynamics Simulation Study of the Association of Lidocainium Docusate and Its Derivatives in Aqueous Solution. Molecular Pharmaceutics, 2015, 12, 1893-1901.	2.3	16
349	Structural characterization of niobium oxide thin films grown on SrTiO3(111) and (La,Sr)(Al,Ta)O3(111) substrates. Journal of Applied Physics, 2016, 120, 245302.	1.1	16
350	Anti-phase boundaries at the SrTiO3/Si(001) interface studied using aberration-corrected scanning transmission electron microscopy. Applied Physics Letters, 2016, 108, .	1.5	16
351	Atomic-resolution structure imaging of defects and interfaces in compound semiconductors. Progress in Crystal Growth and Characterization of Materials, 2020, 66, 100498.	1.8	16
352	Electron Holography. Springer Handbooks, 2019, , 767-818.	0.3	16
353	A transmission and high-resolution electron microscope study of cozonally twinned growth of eutectic silicon in unmodified Al-Si alloys. Journal of Crystal Growth, 1991, 112, 635-643.	0.7	15
354	Transmission electron microscopy observations of magnetic multilayers. Ultramicroscopy, 1992, 47, 375-382.	0.8	15
355	Microstructural study of Mg-doped p-type GaN: Correlation between high-resolution electron microscopy and Raman spectroscopy. Journal of Applied Physics, 1997, 82, 6008-6011.	1.1	15
356	GaAs-substrate-based long-wave active materials with type-II band alignments. Journal of Vacuum Science & Technology an Official Journal of the American Vacuum Society B, Microelectronics Processing and Phenomena, 2001, 19, 1501.	1.6	15
357	Structural and magnetic properties of CoCrPt perpendicular media grown on different buffer layers. Journal of Magnetism and Magnetic Materials, 2002, 247, 153-158.	1.0	15
358	Thermochemical analysis of MgB2 synthesis by molecular-beam epitaxy. Journal of Crystal Growth, 2004, 270, 107-112.	0.7	15
359	Technology Strategy and Innovation: The Use of Derivative Strategies in the Aerospace Industry. Technology Analysis and Strategic Management, 2004, 16, 509-527.	2.0	15
360	Cluster Dynamics: Corporate Strategy, Industry Evolution and Technology Trajectories - A Case Study of the East Midlands Aerospace Cluster. Local Economy, 2006, 21, 362-377.	0.8	15

#	Article	IF	CITATIONS
361	Application of equal-channel angular pressing to Cu–Co alloy with ferromagnetic precipitates. Materials Science & Engineering A: Structural Materials: Properties, Microstructure and Processing, 2006, 417, 149-157.	2.6	15
362	Direct visualization of three-step magnetization reversal of nanopatterned spin-valve elements using off-axis electron holography. Applied Physics Letters, 2009, 94, .	1.5	15
363	Homoepitaxial N-polar GaN layers and HEMT structures grown by rf-plasma assisted molecular beam epitaxy. Journal of Vacuum Science and Technology B:Nanotechnology and Microelectronics, 2012, 30, 02B113.	0.6	15
364	Calculations of flow-induced orientation distributions for analysis of linear dichroism spectroscopy. Soft Matter, 2013, 9, 4977.	1.2	15
365	Band Gap-Engineered Group-IV Optoelectronic Semiconductors, Photodiodes and Prototype Photovoltaic Devices. ECS Journal of Solid State Science and Technology, 2013, 2, Q172-Q177.	0.9	15
366	Effect of indium in Al _{0.65} Ga _{0.35} N/Al _{0.8} Ga _{0.2} N MQWs for the development of deepâ€UV laser structures in the form of gradedâ€index separate confinement heterostructure (GRINSCH). Physica Status Solidi (A) Applications and Materials Science, 2016, 213, 1165-1169.	0.8	15
367	Investigation of defect creation in GaP/Si(0â€⁻0â€⁻1) epitaxial structures. Journal of Crystal Growth, 2018, 503, 36-44.	0.7	15
368	Nanoparticle transport across model cellular membranes: when do solubility-diffusion models break down?. Journal Physics D: Applied Physics, 2018, 51, 294004.	1.3	15
369	Electron beam stimulated nonthermal crystallization of CdS surface layers: Observations by realâ€time atomicâ€resolution electron microscopy. Applied Physics Letters, 1986, 48, 1751-1753.	1.5	14
370	Imaging xâ€ray multilayer structures using crossâ€sectional high resolution electron microscopy. Journal of Applied Physics, 1992, 72, 5165-5171.	1.1	14
371	Chemical Synthesis of Metastable Germaniumâ^'Carbon Alloys Grown Heteroepitaxially on (100) Si. Chemistry of Materials, 1996, 8, 2491-2498.	3.2	14
372	Surface plasmons and breakdown in thin silicon dioxide films on silicon. Journal of Applied Physics, 1998, 84, 1430-1438.	1.1	14
373	Microstructural and micromagnetic characterization of thin film magnetic tunnel junctions. Journal of Applied Physics, 1999, 85, 4815-4817.	1.1	14
374	Spontaneous chemical ordering and exchange bias in epitaxial Mn0.52Pd0.48/Fe(001) bilayers prepared at room temperature. Applied Physics Letters, 2002, 80, 808-810.	1.5	14
375	Ordered domains and boundary structure in Ba(Cd1/3Ta2/3)O3 perovskite dielectrics. Applied Physics Letters, 2004, 84, 3918-3920.	1.5	14
376	Transmission electron microscopy characterization of electrically stressed AlGaN/GaN high electron mobility transistor devices. Journal of Vacuum Science and Technology B:Nanotechnology and Microelectronics, 2012, 30, .	0.6	14
377	Effect of interfacial oxygen on the microstructure of MBE-grown homoepitaxial N-polar GaN. Journal of Crystal Growth, 2015, 409, 14-17.	0.7	14
378	Doing more with less: The flagellar end piece enhances the propulsive effectiveness of human spermatozoa. Physical Review Fluids, 2020, 5, .	1.0	14

#	Article	IF	CITATIONS
379	Atomic Resolution with the Electron Microscope. Interdisciplinary Science Reviews, 1981, 6, 155-165.	1.0	13
380	An investigation of order/disorder in a chromiaâ€doped rutile by highâ€resolution electron microscopy. Journal of Microscopy, 1983, 129, 263-273.	0.8	13
381	Development and applications of a 300 keV ultrahigh-vacuum high-resolution electron microscope. Ultramicroscopy, 1993, 49, 26-36.	0.8	13
382	Heteroepitaxial CdTe(111) grown by MBE on nominally flat and misoriented Si(001) substrates: characterization by electron microscopy and optical methods. Journal of Crystal Growth, 1996, 159, 58-63.	0.7	13
383	Evidence for charge ordering at room temperature inFe3O4. Physical Review B, 1999, 59, R11633-R11636.	1.1	13
384	Use of Pd and Pt buffers to induce soft magnetic properties in Fe70Co30 thin films. Journal of Magnetism and Magnetic Materials, 2004, 269, 212-216.	1.0	13
385	Establishing exchange bias belowTNwith polycrystallineNi0.52Co0.48Oâ^•Cobilayers. Physical Review B, 2005, 72, .	1.1	13
386	Electron microscopy investigation of spark-eroded Ni–Mn–Ga ferromagnetic shape-memory alloy particles. Scripta Materialia, 2007, 56, 593-596.	2.6	13
387	<i>In situ</i> electron holographic analysis of biased Si n+-p junctions. Applied Physics Letters, 2008, 92, .	1.5	13
388	Observation of dodecagon-shape V-defects in GaN/AlInN multiple quantum wells. Applied Physics Letters, 2010, 97, 161902.	1.5	13
389	Exploring aberration-corrected electron microscopy for compound semiconductors. Microscopy (Oxford, England), 2013, 62, S65-S73.	0.7	13
390	Atomic configurations at InAs partial dislocation cores associated with Z-shape faulted dipoles. Scientific Reports, 2013, 3, 3229.	1.6	13
391	Charge control in N-polar InAlN high-electron-mobility transistors grown by plasma-assisted molecular beam epitaxy. Journal of Vacuum Science and Technology B:Nanotechnology and Microelectronics, 2015, 33, .	0.6	13
392	Monolithic integration of perovskites on Ge(001) by atomic layer deposition: a case study with SrHfxTi1-xO3. MRS Communications, 2016, 6, 125-132.	0.8	13
393	Epitaxial growth of barium titanate thin films on germanium via atomic layer deposition. Journal of Crystal Growth, 2017, 476, 6-11.	0.7	13
394	Strain relaxation in low-mismatched GaAs/GaAs1-xSbx/GaAs heterostructures. Acta Materialia, 2019, 162, 103-115.	3.8	13
395	Small-defect clusters in chromia-doped rutiles. Journal of Solid State Chemistry, 1985, 56, 203-210.	1.4	12
396	The real-time growth of atom planes on Ru, Rh and Sn microcrystals observed at atomic resolution. Journal of Crystal Growth, 1988, 89, 165-170.	0.7	12

#	Article	IF	CITATIONS
397	Raman scattering by interface phonons in GaAsâ€AlAs multipleâ€quantumâ€well structures: Correlation between Raman and highâ€resolution electron microscopy results. Journal of Applied Physics, 1991, 70, 418-421.	1.1	12
398	Growth and structural characterization of highly oriented sputter-deposited (111), (110), and (100) Co/Cu superlattices. Applied Physics Letters, 1997, 71, 1480-1482.	1.5	12
399	Microstructure and dielectric properties of Ba(Cd1/3Ta2/3)O3 microwave ceramics synthesized with a boron oxide sintering aid. Journal of Materials Research, 2004, 19, 3526-3533.	1.2	12
400	Nanopillar growth mode by vapor-liquid-solid epitaxy. Applied Physics Letters, 2004, 84, 5302-5304.	1.5	12
401	Remanent states of nanoscale Co ferromagnets having different shapes. Journal of Magnetism and Magnetic Materials, 2006, 303, 237-242.	1.0	12
402	Microstructural characterization of dispersion-strengthened Cu–Ti–Al alloys obtained by reaction milling. Materials Science & Engineering A: Structural Materials: Properties, Microstructure and Processing, 2007, 454-455, 183-193.	2.6	12
403	Assessment of surface damage and sidewall implantation in AlGaN-based high electron mobility transistor devices caused during focused-ion-beam milling. Journal of Applied Physics, 2008, 104, .	1.1	12
404	Controlled growth behavior of chemical vapor deposited Ni nanostructures. Philosophical Magazine, 2012, 92, 2173-2186.	0.7	12
405	Progress and problems for atomic-resolution electron microscopy. Micron, 2012, 43, 504-508.	1.1	12
406	Characterization of structural defects in SnSe2 thin films grown by molecular beam epitaxy on GaAs (111)B substrates. Journal of Crystal Growth, 2016, 453, 58-64.	0.7	12
407	Towards defect-free epitaxial CdTe and MgCdTe layers grown on InSb (001) substrates. Journal of Crystal Growth, 2016, 439, 99-103.	0.7	12
408	Impact of metastable phases on electrical properties of Si with different doping concentrations after processing by high-pressure torsion. Scripta Materialia, 2018, 157, 120-123.	2.6	12
409	High resolution electron microscopy of surfaces and surface reactions. Surface and Interface Analysis, 1987, 10, 135-141.	0.8	11
410	Characterization of thin films, interfaces and surfaces by high-resolution electron microscopy. Ultramicroscopy, 1991, 37, 169-179.	0.8	11
411	Characterization of WCx/B4C multilayers sputtered in reactive argon/methane atmospheres. Thin Solid Films, 1994, 239, 57-70.	0.8	11
412	Strategies for the synthesis of highly concentrated Si1â^'yCy diamond-structured systems. Applied Physics Letters, 1998, 72, 2117-2119.	1.5	11
413	III-N semiconductor growth with activated nitrogen: State-specific study of A3Σu+ metastable N2 molecules. Applied Physics Letters, 2000, 77, 3030-3032.	1.5	11
414	Kinetic control of Ge(Si)â^•Si(100) dome cluster composition. Applied Physics Letters, 2005, 87, 223101.	1.5	11

#	ARTICLE	IF	CITATIONS
415	Growth and characterization of plasma-assisted molecular beam epitaxial-grown AlGaN/GaN heterostructures on free-standing hydride vapor phase epitaxy GaN substrates. Journal of Vacuum Science & Technology an Official Journal of the American Vacuum Society B, Microelectronics Processing and Phenomena, 2005, 23, 1190.	1.6	11
416	Microstructure, magnetotransport, and magnetic properties of Gd-doped amorphous carbon. Physical Review B, 2007, 75, .	1.1	11
417	Fabrication of spherical particles with mixed amorphous/crystalline nanostructured cores and insulating oxide shells. Journal of Materials Research, 2008, 23, 1758-1763.	1.2	11
418	Impact of substrate temperature on the structural and optical properties of strain-balanced InAs/InAsSb type-II superlattices grown by molecular beam epitaxy. Applied Physics Letters, 2013, 102, .	1.5	11
419	A calibration method for group V fluxes and impact of V/III flux ratio on the growth of InAs/InAsSb type-II superlattices by molecular beam epitaxy. Journal of Crystal Growth, 2013, 378, 145-149.	0.7	11
420	Using structural disorder to enhance the magnetism and spin-polarization in FexSi1 â´'xthin films for spintronics. Materials Research Express, 2014, 1, 026102.	0.8	11
421	Spectral identification scheme for epitaxially grown single-phase niobium dioxide. Journal of Applied Physics, 2016, 119, .	1.1	11
422	Zintl layer formation during perovskite atomic layer deposition on Ge (001). Journal of Chemical Physics, 2017, 146, 052817.	1.2	11
423	Strategies for Analyzing Noncommonâ€Atom Heterovalent Interfaces: The Case of CdTeâ€onâ€InSb. Advanced Materials Interfaces, 2020, 7, 1901658.	1.9	11
424	Analysis of high-voltage, high-resolution images of lattice defects in experimentally-deformed dolomite. Physics and Chemistry of Minerals, 1983, 9, 102-108.	0.3	10
425	Characterization of filamentous carbon on Ni/MgO catalysts by high-resolution electron microscopy. Ultramicroscopy, 1990, 34, 54-59.	0.8	10
426	Strain measurements of SiGeC heteroepitaxial layers on Si(001) using ion beam analysis. Journal of Vacuum Science and Technology A: Vacuum, Surfaces and Films, 1996, 14, 441-446.	0.9	10
427	Surfactant-mediated growth of Ge/Si(001) studied by Raman spectroscopy and TEM. Journal of Crystal Growth, 1999, 201-202, 538-541.	0.7	10
428	Enhanced blocking temperature in NiO spin valves: Role of cubic spinel ferrite layer between pinned layer and NiO. Applied Physics Letters, 2000, 77, 1191-1193.	1.5	10
429	Electrical, structural and microstructural characteristics of as-deposited and annealed Pt and Au contacts on chemical-vapor-cleaned GaN thin films. Journal of Applied Physics, 2002, 91, 2133-2137.	1.1	10
430	Growth of Fe/Ge(001) heterostructures by molecular beam epitaxy: Interface structure, electronic and magnetic properties. Journal of Vacuum Science & Technology an Official Journal of the American Vacuum Society B, Microelectronics Processing and Phenomena, 2002, 20, 1586.	1.6	10
431	Electron microscopy studies of epitaxial MgB2 superconducting thin films grown by in situ reactive evaporation. Journal of Crystal Growth, 2005, 280, 602-611.	0.7	10
432	Atomic Resolution Transmission Electron Microscopy of the Microstructure of Ordered Ba(Cd1/3Ta2/3)O3 Perovskite Ceramics. Journal of the American Ceramic Society, 2006, 89, 1047-1052.	1.9	10

#	Article	IF	CITATIONS
433	Effect of shape on magnetic response for slotted Co nanorings. Journal of Applied Physics, 2007, 102, .	1.1	10
434	Optimized thickness of superconducting aluminum electrodes for measurement of spin polarization with MgO tunnel barriers. Applied Physics Letters, 2007, 90, 202502.	1.5	10
435	Growth kinetics of AlN and GaN films grown by molecular beam epitaxy on R-plane sapphire substrates. Journal of Applied Physics, 2010, 108, 043501.	1.1	10
436	Applications of TEM imaging, analysis and electron holography to III-nitride HEMT devices. Microelectronics Reliability, 2010, 50, 1514-1519.	0.9	10
437	Structural properties of InAs/InAs1–xSbx type-II superlattices grown by molecular beam epitaxy. Journal of Vacuum Science and Technology B:Nanotechnology and Microelectronics, 2012, 30, 02B106.	0.6	10
438	MBE-Grown ZnTe/Si, a Low-Cost Composite Substrate. Journal of Electronic Materials, 2012, 41, 2917-2924.	1.0	10
439	Structure and morphology of polar and semi-polar pyramidal surfaces coating wurtzite ZnO micro-wires. Journal of Materials Science, 2013, 48, 3857-3862.	1.7	10
440	Study of InAs/InAsSb type-II superlattices using high-resolution x-ray diffraction and cross-sectional electron microscopy. Journal of Crystal Growth, 2013, 381, 1-5.	0.7	10
441	Characterization of electrical properties in axial Si-Ge nanowire heterojunctions using off-axis electron holography and atom-probe tomography. Journal of Applied Physics, 2016, 120, .	1.1	10
442	Bright-field imaging of compound semiconductors using aberration-corrected scanning transmission electron microscopy. Semiconductor Science and Technology, 2016, 31, 094002.	1.0	10
443	Growth of II-VI/III-V heterovalent quantum structures. Journal of Vacuum Science and Technology B:Nanotechnology and Microelectronics, 2018, 36, .	0.6	10
444	Formation of metastable bc8 phase from crystalline Si0.5Ge0.5 by high-pressure torsion. Materials Characterization, 2020, 169, 110590.	1.9	10
445	Achievement of atomic resolution electron microscopy. Journal of Electron Microscopy Technique, 1989, 12, 11-23.	1.1	9
446	Investigations of microstructure of thin TbFeCo films by highâ€resolution electron microscopy. Journal of Applied Physics, 1991, 69, 6590-6594.	1.1	9
447	High-resolution scanning electron microscopy for the characterization of supported metal catalysts. Catalysis Letters, 1995, 31, 57-64.	1.4	9
448	Crystalline-to-amorphous transition in chemical vapor deposition of pseudomorphic Si1â^'xâ^'yGexCy films. Applied Physics Letters, 1997, 71, 1634-1636.	1.5	9
449	Control of composition and crystallinity in the molecular beam epitaxy of strain-compensated Si1 â^' x â^' yGexCy alloys on Si. Journal of Crystal Growth, 1997, 175-176, 486-492.	0.7	9
450	EELS near-edge structure in the Laves-phase compoundsTiCr2andTiCo2: Theoretical and experimental studies. Physical Review B, 2004, 69, .	1,1	9

#	Article	IF	CITATIONS
451	Microstructural characterization of HgTe/HgCdTe superlattices. Journal of Crystal Growth, 2004, 271, 29-36.	0.7	9
452	Microstructure of interfacial HgTe/CdTe superlattice layers for growth of HgCdTe on CdZnTe (211)B substrates. Journal of Crystal Growth, 2007, 309, 153-157.	0.7	9
453	Introduction: Materials Research in an Aberration-Free Environment. Microscopy and Microanalysis, 2008, 14, 1-1.	0.2	9
454	Measurement of polarization-induced electric fields in GaN/AlInN quantum wells. Applied Physics Letters, 2012, 101, .	1.5	9
455	Band alignment of zinc oxide as a channel layer in a gate stack structure grown by plasma enhanced atomic layer deposition. Journal of Vacuum Science and Technology B:Nanotechnology and Microelectronics, 2012, 30, .	0.6	9
456	TEM Characterization of HgCdTe/CdTe Grown on GaAs(211)B Substrates. Journal of Electronic Materials, 2013, 42, 3142-3147.	1.0	9
457	Determination of Mean Inner Potential and Inelastic Mean Free Path of ZnTe Using Off-Axis Electron Holography and Dynamical Effects Affecting Phase Determination. Microscopy and Microanalysis, 2015, 21, 1406-1412.	0.2	9
458	Effect of proton irradiation energy on AlGaN/GaN metal-oxide semiconductor high electron mobility transistors. Journal of Vacuum Science and Technology B:Nanotechnology and Microelectronics, 2015, 33, 051208.	0.6	9
459	MBE growth of sharp interfaces in dilute-nitride quantum wells with improved nitrogen-plasma design. Journal of Vacuum Science and Technology B:Nanotechnology and Microelectronics, 2015, 33, 031209.	0.6	9
460	Spectrum and phase mapping across the epitaxial γ-Al2O3/SrTiO3 interface. Applied Physics Letters, 2016, 108, .	1.5	9
461	Surface structure analysis of Eu Zintl template on Ge(001). Surface Science, 2018, 674, 94-102.	0.8	9
462	Crystalline SrZrO3 deposition on Ge (001) by atomic layer deposition for high- <i>k</i> dielectric applications. Journal of Applied Physics, 2018, 124, .	1.1	9
463	High-voltage, high-resolution lattice images of dolomite. Nature, 1981, 290, 389-390.	13.7	8
464	Growth and characterization of heteroepitaxial CdTe and ZnTe on Ge(001) buffer layers. Applied Physics Letters, 1996, 69, 2086-2088.	1.5	8
465	Do ballistic channels contribute to the magnetoresistance in magnetic tunnel junctions?. Applied Physics Letters, 2002, 80, 285-287.	1.5	8
466	ChemCatChem: A Catalyst for Communication. ChemCatChem, 2009, 1, 3-4.	1.8	8
467	Influence of Substrate Temperature and Post-Deposition Annealing on Material Properties of Ga-Doped ZnO Prepared by Pulsed Laser Deposition. Journal of Electronic Materials, 2011, 40, 419-428.	1.0	8
468	Microstructural Characterization of CdTe(211)B/ZnTe/Si(211) Heterostructures Grown by Molecular Beam Epitaxy. Journal of Electronic Materials, 2011, 40, 1733-1737.	1.0	8

#	Article	IF	CITATIONS
469	Effect of spacer layer thickness on structural and optical properties of multi-stack InAs/GaAsSb quantum dots. Applied Physics Letters, 2015, 107, 173109.	1.5	8
470	Contradictory nature of Co doping in ferroelectricBaTiO3. Physical Review B, 2016, 94, .	1.1	8
471	Substrateâ€independent analysis of microcrystalline silicon thin films using UV Raman spectroscopy. Physica Status Solidi (B): Basic Research, 2017, 254, 1700204.	0.7	8
472	Adaptive capability and path creation in the post-industrial city: the case of Nottingham's biotechnology sector. Cambridge Journal of Regions, Economy and Society, 2017, 10, 491-508.	1.7	8
473	Sharp Quadrature Error Bounds for the Nearest-Neighbor Discretization of the Regularized Stokeslet Boundary Integral Equation. SIAM Journal of Scientific Computing, 2019, 41, B139-B152.	1.3	8
474	Epitaxial Oxides on Glass: A Platform for Integrated Oxide Devices. ACS Applied Nano Materials, 2019, 2, 7713-7718.	2.4	8
475	Direct Observation of Large Atomic Polar Displacements in Epitaxial Barium Titanate Thin Films. Advanced Materials Interfaces, 2020, 7, 2000555.	1.9	8
476	The observation of amorphous materials at high voltage and high resolution. Journal of Microscopy, 1980, 119, 19-28.	0.8	7
477	High resolution electron microscopy of interfaces in chlorinated phthalocyanine molecular crystals. Journal of Microscopy, 1986, 141, 3-9.	0.8	7
478	Identifying characteristics of the fibrous cesium titanate Cs2Ti5O11. Journal of Solid State Chemistry, 1987, 69, 360-368.	1.4	7
479	Simulations for surface profile imaging. Ultramicroscopy, 1988, 25, 265-277.	0.8	7
480	High resolution imaging of magnetic multilayers. Scripta Metallurgica Et Materialia, 1994, 30, 689-694.	1.0	7
481	X-ray diffraction and high resolution transmission electron microscopy of 3C-SiC/AlN/6H-SiC(0001). Journal of Electronic Materials, 1997, 26, 1389-1393.	1.0	7
482	Growth and characterization of ZnO thin films on GaN epilayers. Journal of Electronic Materials, 2004, 33, 826-832.	1.0	7
483	Switching behavior of nanoscale Co ferromagnetic elements using off-axis electron holography. Journal of Magnetism and Magnetic Materials, 2005, 290-291, 234-237.	1.0	7
484	Interface properties of an AlN/(AlN) x (SiC)1-x /4H-SiC heterostructure. Physica Status Solidi (A) Applications and Materials Science, 2006, 203, 3720-3725.	0.8	7
485	Off-axis electron holographic potential mapping across AlGaAs/AlAs/GaAs heterostructures. Journal of Applied Physics, 2009, 105, 014910.	1.1	7
486	Phase-shifting electron holography for atomic image reconstruction. Journal of Electron Microscopy, 2010, 59, S81-S88.	0.9	7

#	Article	IF	CITATIONS
487	<i>In situ</i> observations of endotaxial growth of CoSi ₂ nanowires on Si(110) using ultrahigh vacuum transmission electron microscopy. Nanotechnology, 2011, 22, 305606.	1.3	7
488	Band alignment of vanadium oxide as an interlayer in a hafnium oxide-silicon gate stack structure. Journal of Applied Physics, 2012, 112, .	1.1	7
489	Microstructural Characterization of HgCdSe Grown by Molecular Beam Epitaxy on ZnTe/Si(112) and GaSb(112) Substrates. Journal of Electronic Materials, 2012, 41, 2852-2856.	1.0	7
490	Atomic-Scale Characterization of II–VI Compound Semiconductors. Journal of Electronic Materials, 2013, 42, 3168-3174.	1.0	7
491	Enhancement of AlGaN/GaN high electron mobility transistors off-state drain breakdown voltage via backside proton irradiation. Journal of Vacuum Science and Technology B:Nanotechnology and Microelectronics, 2014, 32, 021203.	0.6	7
492	Molecular beam epitaxy growth of antimony-based mid-infrared interband cascade photodetectors. Journal of Crystal Growth, 2015, 425, 364-368.	0.7	7
493	Direct detection and measurement of wall shear stress using a filamentous bio-nanoparticle. Nano Research, 2015, 8, 3307-3315.	5.8	7
494	Investigation of dilute-nitride alloys of GaAsNx (0.01 < x < 0.04) grown by MBE o substrates for photovoltaic solar cell devices. Journal of Vacuum Science and Technology B:Nanotechnology and Microelectronics, 2016, 34, .	on GaAs ((0.6	001) 7
495	Observation of compound semiconductors and heterovalent interfaces using aberration-corrected scanning transmission electron microscopy. Journal of Materials Research, 2017, 32, 921-927.	1.2	7
496	Correlation of Etch Pits and Dislocations in As-grown and Thermal Cycle-Annealed HgCdTe(211) Films. Journal of Electronic Materials, 2017, 46, 5007-5019.	1.0	7
497	Recent studies of oxide-semiconductor heterostructures using aberration-corrected scanning transmission electron microscopy. Journal of Materials Research, 2017, 32, 912-920.	1.2	7
498	The Past, Present, and Future of Sustainable Chemistry. ChemSusChem, 2018, 11, 5-10.	3.6	7
499	EuO epitaxy by oxygen scavenging on SrTiO3 (001): Effect of SrTiO3 thickness and temperature. Journal of Applied Physics, 2018, 124, .	1.1	7
500	Effects of growth temperature on electrical properties of GaN/AlN based resonant tunneling diodes with peak current density up to 1.01 MA/cm2. AlP Advances, 2020, 10, .	0.6	7
501	Impact of Individual Structural Defects in GaAs Solar Cells: A Correlative and In Operando Investigation of Signatures, Structures, and Effects. Advanced Optical Materials, 2021, 9, 2001487.	3.6	7
502	Resolving conservation and development tensions in a small island state: A governance analysis of Curieuse Marine National Park, Seychelles. Marine Policy, 2021, 127, 103617.	1.5	7
503	A highâ€resolution electron microscopic study of defects in sodium β′â€â€alumina. Journal of Microscopy, 1983, 130, 203-214.	0.8	6
504	Electron-beam-induced surface reactions in Pd/PdO films. Surface Science, 1991, 250, 90-98.	0.8	6

#	Article	IF	CITATIONS
505	Ordered Structures in Unstrained, Epitaxial Geâ^'Siâ^'C Films. Chemistry of Materials, 1998, 10, 1396-1401.	3.2	6
506	Substitutional C fraction and the influence of C on Si dimer diffusion in Silâ^'yCy alloys grown on (001) and (118) Si. Applied Physics Letters, 2000, 77, 1310-1312.	1.5	6
507	Electron microscopy characterization of Ba(Cd1/3Ta2/3)O3 microwave dielectrics with boron additive. Journal of Materials Research, 2004, 19, 1387-1391.	1.2	6
508	Excess modes and enhanced scattering in rare-earth-doped amorphous silicon thin films. Physical Review B, 2006, 74, .	1.1	6
509	Effect of Alâ^•N flux ratio during nucleation layer growth on the microstructure of GaN films grown by molecular-beam epitaxy. Applied Physics Letters, 2006, 88, 011916.	1.5	6
510	Concentration dependent microstructure and transport properties of the magnetic semiconductor Gd-Si. Journal of Applied Physics, 2007, 101, 093712.	1.1	6
511	Magnetic and transport properties or amorphous <mmi:math xmlns:mml="http://www.w3.org/1998/Math/MathML" display="inline"><mml:mrow><mml:msub><mml:mi mathvariant="normal">Gd<mml:mi>x</mml:mi></mml:mi </mml:msub><mml:msub><mml:mi mathvariant="normal">Ge<mml:mrow><mml:mn>1</mml:mn><mml:mo>â^²</mml:mo><ml:mi>x<!--</td--><td>1.1 mml:mi> <</td><td>6 /mml:mrow></td></ml:mi></mml:mrow></mml:mi </mml:msub></mml:mrow></mmi:math 	1.1 mml:mi> <	6 /mml:mrow>
512	near the metal-insulator transition. Physical Review B, 2007, 76, . Growth and microstructure dependence of electronic and magnetic properties in magnetically doped Gd-Si amorphous semiconductors. Physical Review B, 2007, 75, .	1.1	6
513	Structural Evolution During Formation and Filling of Self-patterned Nanoholes on GaAs (100) Surfaces. Nanoscale Research Letters, 2008, 3, 530-3.	3.1	6
514	Quantitative Analysis of Dopant Distribution and Activation Across p-n Junctions in AlGaAs/GaAs Light-Emitting Diodes Using Off-Axis Electron Holography. IEEE Transactions on Electron Devices, 2009, 56, 1919-1923.	1.6	6
515	Progress & perspectives for atomic-resolution electron microscopy. Materials Today, 2010, 12, 10-16.	8.3	6
516	Inhibiting copper(i) iodide aggregate assembly in the solid state via macrocyclic encapsulation. Dalton Transactions, 2011, 40, 12257.	1.6	6
517	Low temperature growth of high-k Hf–La oxides by remote-plasma atomic layer deposition: Morphology, stoichiometry, and dielectric properties. Journal of Vacuum Science and Technology A: Vacuum, Surfaces and Films, 2012, 30, .	0.9	6
518	The innovation performance of small rural enterprises and cooperatives in Tehran province, Iran. Local Economy, 2012, 27, 183-192.	0.8	6
519	Technological discontinuities, outsiders and social capital: a case study from Formula 1. European Journal of Innovation Management, 2012, 15, 332-350.	2.4	6
520	Nanostructure–Property Control in AlPSi ₃ /Si(100) Semiconductors Using Direct Molecular Assembly: Theory Meets Experiment at the Atomic Level. Chemistry of Materials, 2014, 26, 4092-4101.	3.2	6
521	Optimization of In2Se3/Si(111) Heteroepitaxy To Enable Bi2Se3/In2Se3 Bilayer Growth. Crystal Growth and Design, 2014, 14, 4617-4623.	1.4	6
522	An indirect method of studying band alignments in nBn photodetectors using off-axis electron holography. Applied Physics Letters, 2015, 107, .	1.5	6

#	Article	IF	CITATIONS
523	Defect creation in InGaAs/GaAs multiple quantum wells–I. Structural properties. Journal of Crystal Growth, 2015, 425, 43-48.	0.7	6
524	Domain structure and perpendicular magnetic anisotropy in CoFe/Pd multilayers using off-axis electron holography. Journal of Magnetism and Magnetic Materials, 2015, 388, 16-21.	1.0	6
525	An EELS signal-from-background separation algorithm for spectral line-scan/image quantification. Ultramicroscopy, 2018, 195, 25-31.	0.8	6
526	Passively parallel regularized stokeslets. Philosophical Transactions Series A, Mathematical, Physical, and Engineering Sciences, 2020, 378, 20190528.	1.6	6
527	Changes in band alignment during annealing at 600 °C of ALD Al2O3 on (InxGa1 â~' x)2O3 for xâ€ Journal of Applied Physics, 2020, 127, 105701.	E‰ <u>=</u> 1.1	0.25–0.7⁄
528	Compositional Control and Optimization of Molecular Beam Epitaxial Growth of (Sb ₂ Te ₃) _{1–<i>x</i>} (MnSb ₂ Te ₄) _{<i>x<!--<br-->Magnetic Topological Insulators. Crystal Growth and Design, 2022, 22, 3007-3015.</i>}	i> 1,/s ub>	6
529	Oxidation of bismuth-tungsten bronzes. Journal of Solid State Chemistry, 1984, 53, 101-112.	1.4	5
530	The structure of Bi15Ti9Fe11O57 and related compounds derived by high-resolution electron microscopy. Journal of Solid State Chemistry, 1989, 80, 178-188.	1.4	5
531	Atomic structure of a tilt grain boundary in aluminum by HREM. Scripta Metallurgica Et Materialia, 1990, 24, 1611-1615.	1.0	5
532	REFLECTION ELECTRON MICROSCOPY METHODOLOGY FOR QUANTIFICATION OF CLUSTER GROWTH: INDIUM CLUSTERS ON THE InP(110) SURFACE. Surface Review and Letters, 1997, 04, 655-669.	0.5	5
533	Reflectivity difference spectroscopy study of thin film ZnSe grown on GaAs by molecular beam epitaxy. Journal of Crystal Growth, 1997, 175-176, 328-333.	0.7	5
534	Wet oxidation of amorphous Si0.67Ge0.25C0.08 grown on (100) Si substrates. Journal of Applied Physics, 1998, 83, 2835-2841.	1.1	5
535	Properties of the native oxide in metal/native oxide multilayers (invited). Journal of Applied Physics, 2002, 91, 7526.	1.1	5
536	Nitrogen activated bowing parameter of GaAs1â^'xNx (x⩽1%) obtained from photoreflectance spectra. Solid-State Electronics, 2004, 48, 291-296.	0.8	5
537	Atomic structure of the m-plane AlN/SiC interface. Journal of Crystal Growth, 2009, 311, 1456-1459.	0.7	5
538	Microstructure and field mapping of AlInN-based heterostructures and devices. Physica Status Solidi C: Current Topics in Solid State Physics, 2010, 7, 2436-2439.	0.8	5
539	Influence of temperature ramp on the materials properties of GaSb grown on ZnTe using molecular beam epitaxy. Journal of Vacuum Science and Technology B:Nanotechnology and Microelectronics, 2012, 30, 02B122.	0.6	5
540	193 nm excimer laser lift-off for AlGaN/GaN high electron mobility transistors. Journal of Vacuum Science and Technology B:Nanotechnology and Microelectronics, 2012, 30, 051209.	0.6	5

#	Article	IF	CITATIONS
541	Band alignment of a HfO2-VO2-HfO2 confined well structure on silicon. Journal of Vacuum Science and Technology B:Nanotechnology and Microelectronics, 2014, 32, 011203.	0.6	5
542	Microstructure of Ti/Al/Ni/Au ohmic contacts for N-polar GaN/AlGaN high electron mobility transistor devices. Journal of Vacuum Science and Technology B:Nanotechnology and Microelectronics, 2014, 32, 011201.	0.6	5
543	Polymerase Chain Reaction on a Viral Nanoparticle. ACS Synthetic Biology, 2015, 4, 1316-1325.	1.9	5
544	Structural evolution of dilute magnetic (Sn,Mn)Se films grown by molecular beam epitaxy. Journal of Applied Physics, 2017, 121, 075301.	1.1	5
545	Integration of ferroelectric BaTiO3 with Ge: The role of a SrTiO3 buffer layer investigated using aberration-corrected STEM. Applied Physics Letters, 2017, 110, .	1.5	5
546	Atomic structure of dissociated 60° dislocations in GaAs/GaAs0.92Sb0.08/GaAs heterostructures. Scripta Materialia, 2018, 153, 77-80.	2.6	5
547	Structural breakdown in high power GaN-on-GaN p-n diode devices stressed to failure. Journal of Vacuum Science and Technology A: Vacuum, Surfaces and Films, 2020, 38, 063402.	0.9	5
548	Observations on the structure of amorphous arsenic by high resolution electron microscopy. Journal of Microscopy, 1980, 119, 29-37.	0.8	4
549	Intergrowths and defect structures in Bi ₉ Ti ₃ Fe ₅ O ₂₇ revealed by highâ€resolution electron microscopy. Journal of Microscopy, 1983, 129, 285-293.	0.8	4
550	Microstructural investigations of tin-molybdenum oxides by high-resolution electron microscopy. Journal of Solid State Chemistry, 1985, 58, 342-349.	1.4	4
551	Investigations of Rhâ€based multilayers for soft xâ€ray applications by highâ€resolution electron microscopy. Journal of Applied Physics, 1991, 70, 2905-2910.	1.1	4
552	Morphology of silicon grain boundaries in Sr-modified Al-Si eutectic alloys by HREM. Ultramicroscopy, 1992, 40, 265-270.	0.8	4
553	Dynamic processes at InP(110) surfaces studied by UHV reflection electron microscopy. Surface Science, 1995, 340, 141-152.	0.8	4
554	Optical characterization of ZnMnSSe quaternary alloys for visible light emitting devices. Journal of Crystal Growth, 1996, 159, 50-53.	0.7	4
555	Materials characterization of Si1â^'xâ^'yGexCy/Si superlattice structures. Thin Solid Films, 1997, 308-309, 358-362.	0.8	4
556	Homoepitaxial GaN Layers Studied by Low-Energy Electron Microscopy, Atomic Force Microscopy and Transmission Electron Microscopy. Physica Status Solidi A, 1999, 176, 469-473.	1.7	4
557	4. Electron holography and its application to magnetic materials. Experimental Methods in the Physical Sciences, 2001, , 111-XIII.	0.1	4
558	Evolution of self-assembled Ge/Si(211) islands. Applied Physics Letters, 2001, 79, 4518-4520.	1.5	4

#	Article	IF	CITATIONS
559	Nitrogen-activated bowing of dilute In[sub y]Ga[sub 1â^'y]As[sub 1â^'x]N[sub x] based on photoreflectance studies. Journal of Applied Physics, 2003, 94, 7576.	1.1	4
560	Determination of In concentration in pseudomorphic InxGa1â^'xN quantum wells based on convergent-beam electron diffraction. Applied Physics Letters, 2004, 84, 490-492.	1.5	4
561	Investigation of HgCdTe p-n device structures grown by liquid-phase epitaxy. Journal of Electronic Materials, 2006, 35, 1192-1196.	1.0	4
562	Effects of annealing on amorphous GdxSi1â^'x near the metal-insulator transition. Journal of Applied Physics, 2007, 101, 023908.	1.1	4
563	Remanent states and magnetization reversal of nanopatterned spin-valve elements using off-axis electron holography. Journal of Applied Physics, 2009, 105, 07D517.	1.1	4
564	Vortex Formation During Magnetization Reversal of Co Slotted Nanorings. IEEE Transactions on Magnetics, 2009, 45, 3885-3888.	1.2	4
565	Quantitative dopant profiling of p-n junction in InGaAsâ^•AlGaAs light-emitting diode using off-axis electron holography. Journal of Vacuum Science and Technology B:Nanotechnology and Microelectronics, 2010, 28, C1D11-C1D14.	0.6	4
566	TiAlNiAu contacts for ultrathin AlN/GaN high electron mobility transistor structures. Journal of Applied Physics, 2010, 108, 084513.	1.1	4
567	CdSe/CdTe type-II superlattices grown on GaSb (001) substrates by molecular beam epitaxy. Applied Physics Letters, 2012, 100, .	1.5	4
568	High Technology and Economic Development: The BioCity Nottingham Technology Incubator. International Journal of Entrepreneurship and Innovation, 2012, 13, 301-309.	1.4	4
569	Rational Design of Monocrystalline (InP) _{<i>y</i>} Ge _{5–2<i>y</i>} /Ge/Si(100) Semiconductors: Synthesis and Optical Properties. Journal of the American Chemical Society, 2013, 135, 12388-12399.	6.6	4
570	Linking, leveraging and learning: sectoral systems of innovation and technological catch-up in China's commercial aerospace industry. Global Business and Economics Review, 2014, 16, 349.	0.2	4
571	Measurement of mean inner potential and inelastic mean free path of ZnO nanowires and nanosheet. Materials Research Express, 2015, 2, 105003.	0.8	4
572	Recovery in dc and rf performance of off-state step-stressed AlGaN/GaN high electron mobility transistors with thermal annealing. Applied Physics Letters, 2015, 106, .	1.5	4
573	Investigation of single-layer/multilayer self-assembled InAs quantum dots on GaAs1-xSbx/GaAs composite substrates. Journal of Applied Physics, 2015, 118, .	1.1	4
574	Evaluation of AlGaN/GaN high electron mobility transistors grown on ZrTi buffer layers with sapphire substrates. Journal of Vacuum Science and Technology B:Nanotechnology and Microelectronics, 2016, 34, 051208.	0.6	4
575	Morphological and microstructural stability of N-polar InAlN thin films grown on free-standing GaN substrates by molecular beam epitaxy. Journal of Vacuum Science and Technology A: Vacuum, Surfaces and Films, 2016, 34, .	0.9	4

576 Transmission electron microscopy and high resolution electron microscopy studies of shallow (Rp $\hat{a}^{1}/420$) Tj ETQq0 0.0 rgBT / \hat{S} verlock 10 1.5 rgBT / \hat{S} verlock 10 rgBT / \hat{S} verl

#	Article	IF	CITATIONS
577	Extended Defects in Deformed Rutile. Physica Status Solidi A, 1985, 89, 559-570.	1.7	3
578	Electron-beam-stimulated processes at CdS surfaces observed by real-time atomic-resolution electron microscopy. Journal of Materials Research, 1986, 1, 560-563.	1.2	3
579	HREM study of structure of supported Pt catalysts. Zeitschrift Für Physik D-Atoms Molecules and Clusters, 1993, 26, 79-81.	1.0	3
580	HREM study of 45° [100]quasiperiodic grain boundary in aluminum. Scripta Materialia, 1996, 35, 327-331.	2.6	3
581	Molecular beam epitaxial growth of ZnSe on GaAs substrates: influence of precursors on interface quality. Journal of Crystal Growth, 1997, 175-176, 613-618.	0.7	3
582	Structural properties of heteroepitaxial germanium-carbon alloys grown on Si (100). Philosophical Magazine A: Physics of Condensed Matter, Structure, Defects and Mechanical Properties, 2001, 81, 1613-1624.	0.8	3
583	Surfactant-mediated growth and characterization of Ge(211)/Si(211) heterostructures grown by molecular beam epitaxy. Journal of Vacuum Science & Technology an Official Journal of the American Vacuum Society B, Microelectronics Processing and Phenomena, 2001, 19, 1562.	1.6	3
584	Structural characterization of base/collector interfaces for magnetic tunnel transistors grown on Si(001). Journal of Applied Physics, 2005, 97, 104514.	1.1	3
585	In situ pendeoepitaxy of GaN using heteroepitaxial AlGaNâ^•GaN cracks. Applied Physics Letters, 2006, 89, 024103.	1.5	3
586	Epitaxial growth of CdTe on (211) silicon mesas formed by deep reactive ion etching. Journal of Electronic Materials, 2006, 35, 1636-1640.	1.0	3
587	Optical and structural characterization of GaN/AlGaN quantum wells for intersubband device applications. Physica Status Solidi C: Current Topics in Solid State Physics, 2010, 7, 2394-2397.	0.8	3
588	InAs/InAsSb Type-II superlattice: a promising material for mid-wavelength and long-wavelength infrared applications. Proceedings of SPIE, 2012, , .	0.8	3
589	Sequential tunneling transport in GaN/AlGaN quantum cascade structures. Physica Status Solidi C: Current Topics in Solid State Physics, 2012, 9, 588-591.	0.8	3
590	Molecular beam epitaxial growth of high-reflectivity and broad-bandwidth ZnTe/GaSb distributed Bragg reflectors. Journal of Vacuum Science and Technology B:Nanotechnology and Microelectronics, 2013, 31, .	0.6	3
591	Epitaxial Zintl aluminide SrAl4grown on a LaAlO3substrate. Physical Review B, 2013, 88, .	1.1	3
592	â€~Beyond the golden triangle': Biotechnology incubation in the East Midlands region of the UK. Local Economy, 2013, 28, 66-84.	0.8	3
593	Atomic-scale characterization of (mostly zincblende) compound semiconductor heterostructures. Journal of Physics: Conference Series, 2013, 471, 012005.	0.3	3
594	Characterization of a-plane GaN templates grown by HVPE and high efficiency deep UV emitting AlGaN/AlN MQWs grown by MBE on such templates. Physica Status Solidi C: Current Topics in Solid State Physics, 2014, 11, 585-589.	0.8	3

#	Article	IF	CITATIONS
595	Nottingham Express Transit. International Journal of Entrepreneurship and Innovation, 2018, 19, 56-68.	1.4	3
596	Molecular beam epitaxial growth and structural properties of hetero-crystalline and heterovalent PbTe/CdTe/InSb structures. Journal of Applied Physics, 2019, 126, .	1.1	3
597	Growth Habits of Bismuth Selenide (Bi ₂ Se ₃) Layers and Nanowires over Stranski–Krastanov Indium Arsenide Quantum Dots. Crystal Growth and Design, 2019, 19, 6989-6993.	1.4	3
598	Strain-dependence of χ(2) in thin film barium strontium titanate. AIP Advances, 2019, 9, .	0.6	3
599	Microstructural Characterization of Defects and Chemical Etching for HgCdSe/ZnTe/Si (211) Heterostructures. Journal of Electronic Materials, 2019, 48, 571-582.	1.0	3
600	Dielectric breakdown in epitaxial BaTiO3 thin films. Journal of Vacuum Science and Technology B:Nanotechnology and Microelectronics, 2020, 38, 044007.	0.6	3
601	Investigation of polycrystalline GaxIn1 â^' xP for potential use as a solar cell absorber with tunable bandgap. Journal of Applied Physics, 2020, 127, 073102.	1.1	3
602	Atomic-Resolution Structure Imaging of Misfit Dislocations at Heterovalent II–VI/III–V Interfaces. ACS Applied Electronic Materials, 2021, 3, 2573-2579.	2.0	3
603	Magnesium-silicide-based multilayers for soft x-ray optics. , 1992, 1546, 502.		2
604	Reflection electron microscopy studies of GaP(110) surfaces in UHV-TEM. Surface Science, 1993, 287-288, 1062-1066.	0.8	2
605	Correlation of electronic and structural properties of MBE-grown AlGaN/GaN heterostructures to Al/N flux ratio during nucleation layer growth. Physica Status Solidi C: Current Topics in Solid State Physics, 2005, 2, 2212-2215.	0.8	2
606	Correlation of microstructure and magnetic properties for exchange-biased Co ferromagnets grown above and below the diluted antiferromagnet Co(Mg)O. Journal of Applied Physics, 2007, 102, 123904.	1.1	2
607	High-resolution imaging of 1:1 [0001] ordered a-plane Al0.3Ga0.7N. Journal of Crystal Growth, 2009, 311, 4162-4166.	0.7	2
608	Conduction electron scattering and spin-flipping at sputtered Al/Cu Interfaces. Journal of Applied Physics, 2011, 109, .	1.1	2
609	Structural properties of InAs/InAs 1-x Sb x type-II superlattices. Proceedings of SPIE, 2012, , .	0.8	2
610	Comparison of microstructure of N-polar GaN/AlGaN/GaN heterostructures grown on different substrates. Journal of Crystal Growth, 2012, 357, 25-29.	0.7	2
611	Impact of dynamical scattering on quantitative contrast for aberration-corrected transmission electron microscope images. Micron, 2016, 89, 77-86.	1.1	2
612	Can Simple Interaction Models Explain Sequence-Dependent Effects in Peptide Homodimerization?. Journal of Physical Chemistry B, 2017, 121, 5928-5943.	1.2	2

#	Article	IF	CITATIONS
613	A Perfect Ten. ChemSusChem, 2017, 10, 2-5.	3.6	2
614	AlGaN/GaN High Electron Mobility Transistor Grown and Fabricated on ZrTi Metallic Alloy Buffer Layers. ECS Journal of Solid State Science and Technology, 2017, 6, S3078-S3080.	0.9	2
615	BIOLOGICAL FLUID MECHANICS UNDER THE MICROSCOPE: A TRIBUTE TO JOHN BLAKE. ANZIAM Journal, 2018, 59, 416-442.	0.3	2
616	<i>(Invited)</i> Comparison of High Voltage, Vertical Geometry Ga ₂ O ₃ Rectifiers with GaN and SiC. ECS Transactions, 2019, 92, 15-24.	0.3	2
617	A hyperspectral unmixing framework for energy-loss near-edge structure analysis. Ultramicroscopy, 2020, 218, 113096.	0.8	2
618	DC and dynamic switching characteristics of field-plated vertical geometry [beta]-Ga2O3 rectifiers. , 2019, , .		2
619	The segregation of molybdenum to twin boundaries in molybdenum-doped tin(IV) oxide. Journal of the Chemical Society Chemical Communications, 1984, , 1483.	2.0	1
620	Investigations of microstructure of thin TbFeCo films by highâ€resolution electron microscopy (abstract). Journal of Applied Physics, 1990, 67, 5954-5954.	1.1	1
621	Tungsten/boron nitride multilayers for XUV optical applications. , 1992, , .		1
622	Characterization of WC x /B 4 C multilayers sputtered in argon/methane atmospheres. , 1993, 1742, 354.		1
623	Electron Crystallography of Room Temperature Charge Ordering in Fe3O4. Microscopy and Microanalysis, 2000, 6, 400-402.	0.2	1
624	Fabrication and characterization of C implantation standards for Si[sub 1â^'xâ^'y]Ge[sub x]C[sub y] alloys. Journal of Vacuum Science and Technology A: Vacuum, Surfaces and Films, 2001, 19, 2879.	0.9	1
625	Introduction: The Otto Scherzer Special Issue on Aberration-Corrected Electron Microscopy. Microscopy and Microanalysis, 2010, 16, 365-365.	0.2	1
626	Intersubband device applications of nitride quantum structures. , 2010, , .		1
627	ChemCatChem: Looking To The Future. ChemCatChem, 2010, 2, 3-4.	1.8	1
628	<i>ChemCatChem</i> : For a Catalytic Future. ChemCatChem, 2011, 3, 4-5.	1.8	1
629	Effect of the Source Field Plate on AlGaN/GaN High Electron Mobility Transistors during Off-State Stress. ECS Transactions, 2011, 41, 41-49.	0.3	1
630	Shape transition and migration of TiSi2 nanostructures embedded in a Si matrix. Journal of Applied Physics, 2011, 110, 094304.	1.1	1

#	Article	IF	CITATIONS
631	<i>ACS Catalysis</i> Wins PROSE Award, Awards 2013 Lectureship for the Advancement of Catalytic Science, and Welcomes New Associate Editor. ACS Catalysis, 2013, 3, 428-428.	5.5	1
632	Epitaxial growth: Phenomenological model of defect creation. , 2014, , .		1
633	High quality MBE grown dilute nitride quantum wells with novel Nitrogen-plasma source design. , 2014, , .		1
634	Atomic Scale Studies of Structure and Bonding in A1PSi3 Alloys Grown Lattice-matched on Si(001). Microscopy and Microanalysis, 2014, 20, 524-525.	0.2	1
635	Continuous control of spin polarization using a magnetic field. Applied Physics Letters, 2016, 108, 212401.	1.5	1
636	Plasma Enhanced Atomic Layer-etched and Regrown GaN-on-GaN High Power <i>p-n</i> Diodes. Microscopy and Microanalysis, 2020, 26, 840-842.	0.2	1
637	Layered two-dimensional selenides and tellurides grown by molecular beam epitaxy. , 2020, , 235-269.		1
638	A Fresh Look at Sustainable Chemistry. ChemSusChem, 2021, 14, 5-9.	3.6	1
639	Biological fluid mechanics under the microscope: a tribute to John Blake. ANZIAM Journal, 0, 59, 416.	0.0	1
640	The Role of the Double-Layer Potential in Regularised Stokeslet Models of Self-Propulsion. Fluids, 2021, 6, 411.	0.8	1
641	Suppressed recovery of functionally important branching Acropora drives coral community composition changes following mass bleaching in Indonesia. Coral Reefs, 2022, 41, 1337-1350.	0.9	1
642	Identification of an electronâ€beamâ€induced reaction product in the praseodymium oxide system. Journal of Microscopy, 1989, 153, 31-37.	0.8	0
643	Recent studies of thin films and surfaces by high-Resolution electron microscopy. Metallurgical and Materials Transactions A - Physical Metallurgy and Materials Science, 1992, 23, 1063-1070.	1.4	0
644	Microstructural and Chemical Characterization of the Inconel/Ti(N) Thin Film and Multilayer System. Journal of X-Ray Science and Technology, 1995, 5, 121-158.	0.7	0
645	Application of chemically enhanced vapour etching in the fabrication on nanostructures. Semiconductor Science and Technology, 1998, 13, A63-A66.	1.0	0
646	MBE Growth and Ultrahigh Temperature Processing of High-Quality AlN Films. Materials Research Society Symposia Proceedings, 1999, 587, 07.12.1.	0.1	0
647	Step Bunching, Chemical Ordering, and Diffusivity in Si1â^'yCy Heteroepitaxy. Materials Research Society Symposia Proceedings, 2000, 618, 65.	0.1	0
648	Ordered Structures in Ba(Cd1/3Ta2/3)O3 Microwave Ceramics: A Transmission Electron Microscopy Study. Materials Research Society Symposia Proceedings, 2003, 783, 5121.	0.1	0

#	Article	IF	CITATIONS
649	Nanoscale Structural and Magnetic Characterization Using Electron Microscopy. , 2006, , 119-145.		0
650	Oxidation behavior of In[sub 95]Sn[sub 5] solid solution. Journal of Vacuum Science & Technology B, 2008, 26, 1670.	1.3	0
651	Intersubband transitions in GaN-based quantum wells: a new materials platform for infrared device applications. Proceedings of SPIE, 2010, , .	0.8	Ο
652	Microstructural Characterization of CdTe Surface Passivation Layers. Journal of Electronic Materials, 2010, 39, 924-929.	1.0	0
653	Investigation of the main correlations between structural and physical propertiess of InAs quantum dots, embedded between strain-relief GaAsSb layers. , 2011, , .		Ο
654	Structural characterization of III-nitride materials and devices. Proceedings of SPIE, 2011, , .	0.8	0
655	Electric Field Driven Degradation of AlGaN/GaN High Electron Mobility Transistors during Off-State Stress. ECS Transactions, 2011, 41, 89-100.	0.3	Ο
656	Study of uniformity of high performance AlInN HEMT with ultraâ€ŧhin barrier. Physica Status Solidi C: Current Topics in Solid State Physics, 2011, 8, 2081-2085.	0.8	0
657	Growth and Material Properties of ZnTe/GaSb Heterostructures for Optoelectronic Device Applications. , 2012, , .		О
658	Improving the Spatial Resolution of Atomic-Scale EDS Mapping for Chemical Imaging and Quantification of Metallic Alloy Structures. Microscopy and Microanalysis, 2014, 20, 130-131.	0.2	0
659	Microscopic Investigation of Mono-layer/Multi-layer self-assembled InAs QDs on GaAs1-xSbx/GaAs Composite Substrates for Photovoltaic Solar Cells. Microscopy and Microanalysis, 2014, 20, 554-555.	0.2	0
660	Structural and optical properties of multi-stack InAs/GaAsSb quantum dots with different Sb composition. , 2014, , .		0
661	InGaAs/GaAs MQWs: Correlation of crystal and physical properties. , 2014, , .		О
662	Interface engineered wetting-layer-free InAs quantum dots on GaAs(001). , 2015, , .		0
663	The scientific careers of Robert Sinclair and Nestor Zaluzec - A brief sketch. Ultramicroscopy, 2017, 176, 2-4.	0.8	О
664	Microscale magnetic compasses. Journal of Applied Physics, 2017, 122, .	1.1	0
665	Properties and Imaging of Thick Doped Amorphous Silicon in Direct Contact with Aluminum For Use in Silicon Heterojunction Solar Cells. , 2018, , .		0
666	A Big Year for Chemistry and Sustainability. ChemSusChem, 2019, 12, 343-346.	3.6	0

#	Article	IF	CITATIONS
667	Approaches to Phase Imaging in the Electron Microscope. Microscopy and Microanalysis, 2020, 26, 1546-1546.	0.2	0
668	Annealing Effects on the Band Alignment of ALD SiO ₂ on (In _x Ga _{1â^`x}) ₂ O ₃ for x = 0.25–0.74. ECS Journal of Solid State Science and Technology, 2020, 9, 045001.	0.9	0
669	Lucky Thirteen. ChemSusChem, 2020, 13, 6-10.	3.6	0
670	Knocking on the door: policy, agency and path creation in the post-industrial city. European Planning Studies, 2021, 29, 899-922.	1.6	0
671	Heads and Tails: Requirements for Informative and Robust Computational Measures of Sperm Motility. , 2021, , 135-150.		0
672	Structural characterization of III-nitrides using electron microscopy. , 2007, , .		0
673	The Making of Innovative Entrepreneurs in Business Schools in a Resource Constrained Environment. Proceedings - Academy of Management, 2020, 2020, 19277.	0.0	0
674	Keeping it Green. ChemSusChem, 2022, 15, e202102612.	3.6	0
675	InAs/InAs1-xSbx Superlattices on GaSb Substrates: A Promising Material System for Mid- and Long-Wavelength Infrared Detectors. , 0, , .		0